Cell Reports

Article

# Purkinje-cell-specific MeCP2 deficiency leads to motor deficits and autistic-like behavior due to aberrations in PTP1B-TrkB-SK signaling

## Graphical abstract

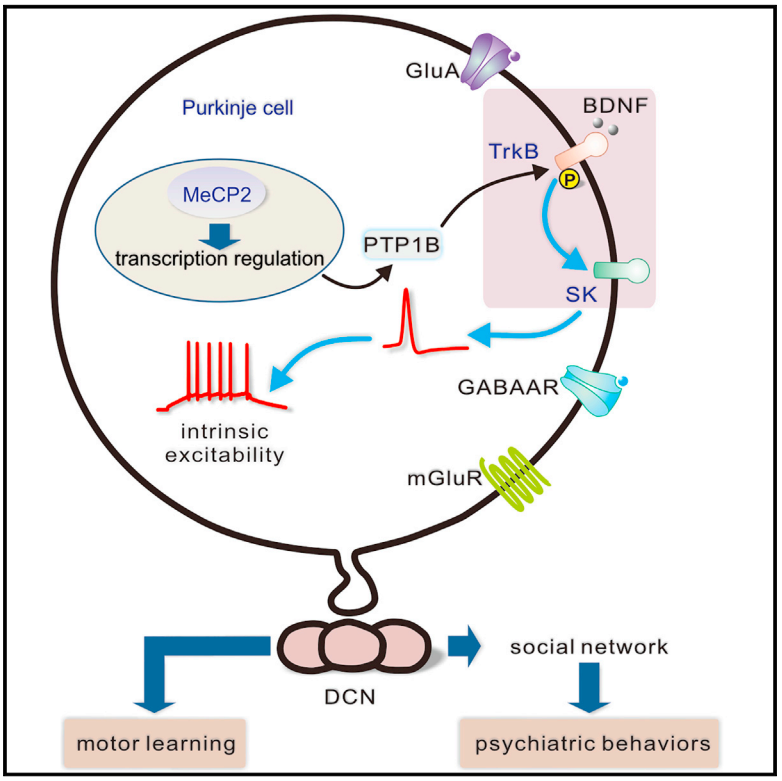


## Authors

Fang-Xiao Xu, Xin-Tai Wang, Xin-Yu Cai, ..., Chris De Zeeuw, Lin Zhou, Ying Shen

## Correspondence

c.dezeeuw@erasmusmc.nl (C.D.Z.), lynchow@zju.edu.cn (L.Z.), yshen@zju.edu.cn (Y.S.)

## In brief

Xu et al. show that the PTP1B-TrkB-SK signaling cascade controls the intrinsic excitability of Purkinje cells and that MeCP2 deficiency alters this cascade and causes motor deficits as well as autistic-like behaviors. Expressing TrkB$^{Y706E}$ rescues the excitability of Purkinje cells, motor learning, and autistic behavior of *Mecp2* mutant mice.

## Highlights

- PTP1B-TrkB-SK signaling cascade controls intrinsic excitability of PCs
- MeCP2 deficiency in PCs alters the cascade and causes motor deficits and autistic behaviors
- Expressing TrkB$^{Y706E}$ reduces SK2 currents and restores excitability of PCs
- Expressing TrkB$^{Y706E}$ in PCs rescues motor and autistic behaviors of *Mecp2* mutant mice

Xu et al., 2023, Cell Reports *42*, 113559
December 26, 2023 
https://doi.org/10.1016/j.celrep.2023.113559

CellPress

Cell Reports

CellPress
OPEN ACCESS

Article

# Purkinje-cell-specific MeCP2 deficiency leads to motor deficits and autistic-like behavior due to aberrations in PTP1B-TrkB-SK signaling

Fang-Xiao Xu,[1,8] Xin-Tai Wang,[1,2,8] Xin-Yu Cai,[1] Jia-Yu Liu,[1] Jing-Wen Guo,[1] Fan Yang,[3] Wei Chen,[1] Martijn Schonewille,[4] Chris De Zeeuw,[4,5,*] Lin Zhou,[1,*] and Ying Shen[1,6,7,9,*]

[1]Department of Physiology and Department of Psychiatry, Sir Run Run Shaw Hospital, Zhejiang University School of Medicine, Hangzhou 310000, China
[2]Institute of Life Sciences, College of Life and Environmental Sciences, Hangzhou Normal University, Hangzhou 311121, China
[3]Department of Biophysics, Zhejiang University School of Medicine, Hangzhou 310058, China
[4]Department of Neuroscience, Erasmus University Medical Center, 3000 DR Rotterdam, the Netherlands
[5]The Netherlands Institute for Neuroscience, Royal Dutch Academy of Arts and Science, 1105 CA Amsterdam, the Netherlands
[6]International Institutes of Medicine, Fourth Affiliated Hospital, Zhejiang University School of Medicine, Yiwu 322000, China
[7]Key Laboratory of Medical Neurobiology of Zhejiang Province, Zhejiang University School of Medicine, Hangzhou 310000, China
[8]These authors contributed equally
[9]Lead contact
*Correspondence: c.dezeeuw@erasmusmc.nl (C.D.Z.), lynchow@zju.edu.cn (L.Z.), yshen@zju.edu.cn (Y.S.)
https://doi.org/10.1016/j.celrep.2023.113559

## SUMMARY

Patients with Rett syndrome suffer from a loss-of-function mutation of the *Mecp2* gene, which results in various symptoms including autistic traits and motor deficits. Deletion of *Mecp2* in the brain mimics part of these symptoms, but the specific function of methyl-CpG-binding protein 2 (MeCP2) in the cerebellum remains to be elucidated. Here, we demonstrate that *Mecp2* deletion in Purkinje cells (PCs) reduces their intrinsic excitability through a signaling pathway comprising the small-conductance calcium-activated potassium channel PTP1B and TrkB, the receptor of brain-derived neurotrophic factor. Aberration of this cascade, in turn, leads to autistic-like behaviors as well as reduced vestibulocerebellar motor learning. Interestingly, increasing activity of TrkB in PCs is sufficient to rescue PC dysfunction and abnormal motor and non-motor behaviors caused by *Mecp2* deficiency. Our findings highlight how PC dysfunction may contribute to Rett syndrome, providing insight into the underlying mechanism and paving the way for rational therapeutic designs.

## INTRODUCTION

Over the past decades, the relevance of the ''cerebellar connectome'' has been emerging.[1] The cerebellum is heavily connected with other brain regions, including the thalamus and cerebral cortex,[2,3] subserving not only motor but also non-motor functions.[4,5] Genetic mutations leading to aberrations in cerebellocerebral connectivity result in diseases with mental dysfunction, such as autism spectrum disorder (ASD),[6] in which developmental and functional disruptions in the cerebellar connectome can affect social interactions and experiences of reward.[7–13]

Rett syndrome patients suffer from loss-of-function mutations of the *Mecp2* gene encoding methyl-CpG-binding protein 2 (MeCP2).[14] Loss of *Mecp2* function causes not only typical ASD features, such as deficits in social interaction and repetitive behavior, but also motor symptoms, such as ataxia and tremors.[15,16] In mice, global loss of *Mecp2* causes deficits in motor performance, including hindlimb clasping, hypoactivity, and tremors.[17] To date, many Rett syndrome symptoms have been attributed to cellular deficits in various brain regions, such as the cerebral cortex and basal ganglia,[18–22] but surprisingly, the impact of *Mecp2* mutation in the main output neurons of the cerebellar cortex, Purkinje cells (PCs), has been relatively neglected. Moreover, the pathological consequences of MeCP2 mutation at the molecular and cellular levels that ultimately lead to changes in behavior have yet to be fully established.

Utilizing a mouse model with PC-specific deletion of *Mecp2*, we here shed light on the impact of loss of function of MeCP2 at both the cellular and behavioral levels. Our results demonstrate that deletion of *Mecp2* reduces the excitability of PCs through a signaling pathway, which entails the PTP1B-TrkB (the receptor of brain-derived neurotrophic factor [BDNF]) cascade. These PC-specific cellular changes, in turn, lead to aberrations in both motor and non-motor behaviors. Moreover, increasing the activity of TrkB in PCs at the adult stage is sufficient to rescue PC dysfunction and defective behaviors caused by *Mecp2* deficiency. In short, our findings elucidate part of the pathogenetic mechanisms underlying Rett syndrome and highlight how PC dysfunction may contribute to symptoms associated with ASD.

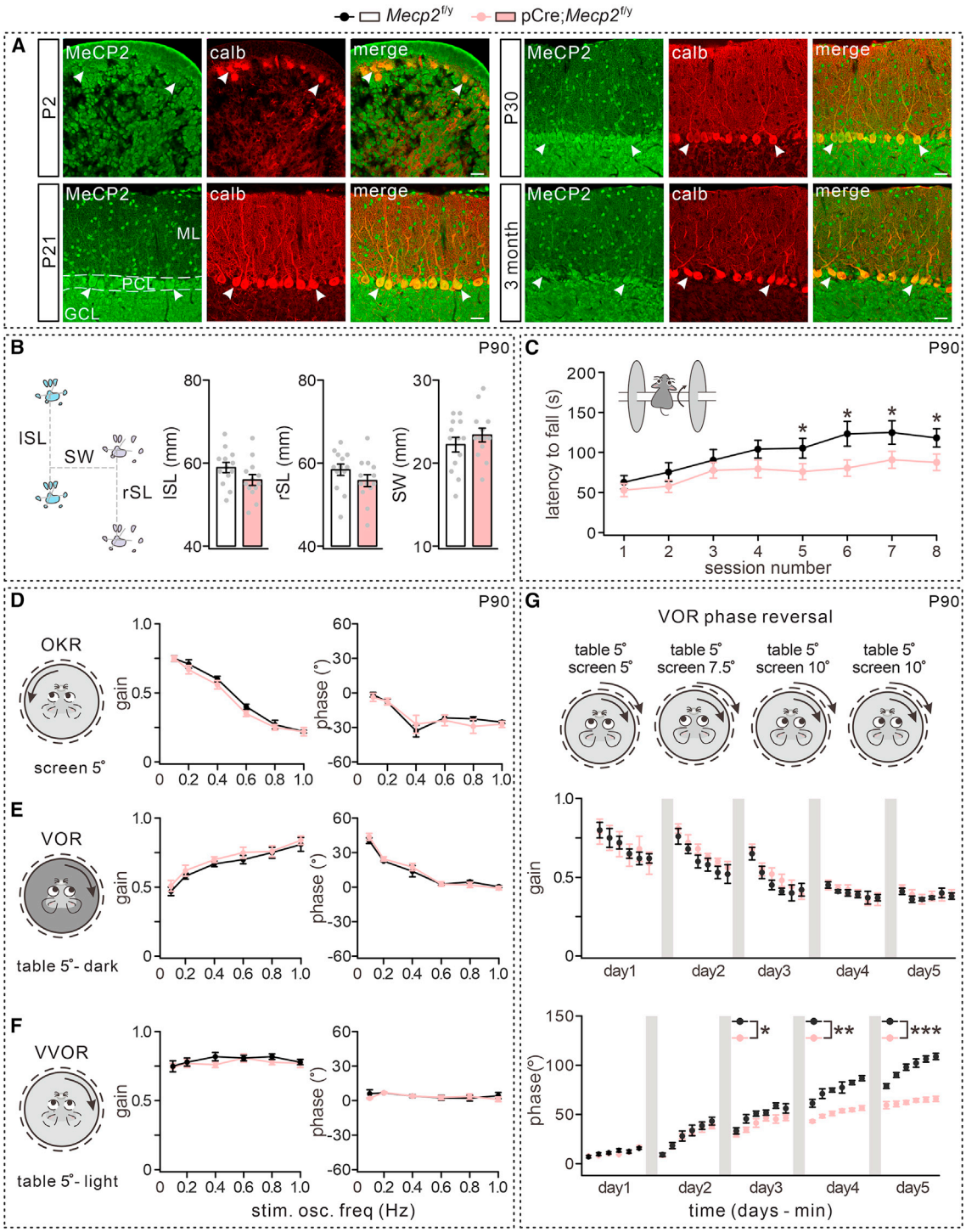


**Figure 1. Impaired motor learning in pCre;*Mecp2*$^{f/y}$ mice (P90)**

(A) MeCP2 was expressed in PCs (arrows). Scale bar, 20 μm calb, calbindin; ML, molecular layer; PCL, Purkinje cell layer; GCL, granule cell layer.

(B) Footprints of *Mecp2*$^{f/y}$ and pCre;*Mecp2*$^{f/y}$ mice at P90 (n = 13 for each group). ISL, left step width; rSL, right step width; SW, stance width.

(C) Time spent on the rotarod (n = 13 for each group).

(D) Gains and phases in OKR.

(E) Gains and phases in VOR.

*(legend continued on next page)*

## RESULTS

### *Mecp2* deletion in PCs impairs motor learning

Consistent with previous work,[23] we found that MeCP2 is robustly expressed in PCs of post-natal mice (post-natal day 2 [P2]–P90) (Figure 1A). To determine the role of MeCP2 in PCs, mice with a *Mecp2* deletion specifically in PCs (pCre;*Mecp2*$^{f/f}$ and pCre;*Mecp2*$^{f/y}$) were generated by crossing pCP2-Cre with *Mecp2*$^{f/f}$ (female) or *Mecp2*$^{f/y}$ (male) mice. *Mecp2* deletion was confirmed by assessing its mRNA in PCs (Figure S1A). Body weight and cerebellar size of *Mecp2* conditional knockout (cKO) mice appeared normal at both P30 and P90 (Figures S1B and S1C).

We asked whether PC deletion of *Mecp2* leads to motor deficits. During the footprint test, cKO mice exhibited normal gait (Figure 1B). In the rotarod test, cKO mice showed limited improvement and learning over 8 sessions; their latency to fall was shorter than that of control mice at late stages (Figure 1C). Next, we examined compensatory eye movements, which are more specific to the function of the cerebellum. We found that the amplitude (gain) and timing (phase) of the baseline optokinetic reflex (OKR), vestibulo-ocular reflex (VOR), and visually enhanced VOR (VVOR) did not differ between control and cKO mice (Figures 1D–1F), supporting the hypothesis that PC deletion of *Mecp2* does not alter basic motor performance. We continued to test a phase-reversal VOR adaptation protocol, a more sensitive test for cerebellar learning.[10,24] While both control and cKO mice did not differ in VOR gain decrease, this training resulted in an increase in VOR phase in control mice that could not be matched by cKO mice (day 3, $p = 0.02$; day 4, $p = 0.002$; day 5, $p < 0.001$; $n = 12$/group; ANOVA repeated measures) (Figure 1G). Together, these results indicate that PC deletion of *Mecp2* impairs motor learning.

### Abnormal social and repetitive behaviors in cKO mice

Mutant mice with PC-specific deletion of autism-related genes exhibit autistic-like behaviors.[7–10,13] Thus, we examined psychiatric behaviors in female (pCre;*Mecp2*$^{f/f}$) and male (pCre;*Mecp2*$^{f/y}$) mice because functional magnetic resonance imaging (fMRI) scanning in ASD patients shows sex-dependent differences in cortico-cerebellar organization.[25] In the three-chamber interaction task, pCre;*Mecp2*$^{f/y}$ and pCre;*Mecp2*$^{f/f}$ mice displayed a preference for a stranger mouse (S1), similar to *Mecp2*$^{f/y}$ and *Mecp2*$^{f/f}$ mice (Figure 2A). Moreover, there was no difference in the sniffing time between *Mecp2*$^{f/y}$ and pCre;*Mecp2*$^{f/y}$ mice or between *Mecp2*$^{f/f}$ and pCre;*Mecp2*$^{f/f}$ mice (Figure 2A). These results indicate that mutant mice have no deficit in social ability. We next tested social novelty by introducing a second stranger mouse (S2). Both *Mecp2*$^{f/y}$ and *Mecp2*$^{f/f}$ mice demonstrated an increased preference for S2, whereas neither pCre;*Mecp2*$^{f/y}$ nor pCre;*Mecp2*$^{f/f}$ mice showed a particular preference for S2 (Figure 2A).

These observations were further examined by performing the resident-intruder test.[26] In trial 1, a subject mouse was exposed to an unfamiliar mouse for an interaction of 5 min. After a 1-h inter-trial interval, either the previous familiar mouse or a second novel mouse was introduced to the subject mouse in trial 2 (Figures S2A and S2B). We found a significant reduction in the exploration time for control mice, but not cKO mice, in trial 2. In comparison, both control and cKO mice showed no differences in exploring the novel mouse (Figures S2A and S2B). Combined with the three-chamber test, these results suggested that cKO mice may have impaired social memory.

Repetitive behavior was examined using the grooming, marble burying, and T maze tasks. Water spray[10] induced grooming behaviors in pCre;*Mecp2*$^{f/y}$ and pCre;*Mecp2*$^{f/f}$ mice, as shown by more interrupted bouts and time spent self-grooming (Figure 2B). In contrast, no difference was observed in the number of buried marbles between control and cKO mice (Figure 2C). Moreover, cKO mice showed no difference in the T maze task test compared with controls (Figure 2D).

Last, we investigated whether the deficit in social function may be due to impaired ability to recognize odorants. Thus, we performed odorant cue recognition experiments and found that cKO mice displayed reduced interest when exposed repeatedly to the same odorant (Figures S2C and S2D). In this test, cKO mice behaved in a manner similar to control mice, suggesting that cKO mice retained normal olfactory discrimination ability.

Together, our results indicate that both male and female mice with a PC-specific deletion of *Mecp2* exhibit a social novelty defect.

### *Mecp2* deficiency in PCs does not affect cyto-architecture and neurotransmission

As for cerebellar development, *Mecp2* deletion did not interrupt the formation of cerebellar lobules at P30 (Figure S3A). Moreover, the PC layer appeared normal in cKO mice (Figure S3B). Finally, Golgi apparatus staining and Sholl analysis showed that both the intersection number (Figures S3C and S3D) and spine formation were normal in cKO PCs (Figures S3E and S3F). In summary, no evidence supports the hypothesis that *Mecp2* deficiency influences PC morphology.

Previous work suggests that synaptic efficacy and excitatory-inhibitory input balance are affected in mice with *Mecp2* mutations.[22,27] Hence, we investigated whether excitatory and/or inhibitory transmissions of PCs are influenced by *Mecp2* deletion. Using whole-cell patch recordings in cerebellar slices, excitatory and inhibitory inputs of PCs were examined (Figure S4A). First, neither frequency nor amplitude of miniature excitatory postsynaptic currents (mEPSCs) was altered in cKO mice (Figure S4B). Second, neither amplitude nor paired-pulse facilitation (PPF) of evoked (parallel fiber) PF-EPSCs was different between control and cKO mice (Figure S4C). Third, no difference in the amplitude or paired-pulse depression (PPD) of climbing fiber (CF)-EPSCs was found between control and cKO mice (Figure S4D). With applying sub- or suprathreshold stimuli, CF-EPSCs were elicited in an all-or-none fashion in

(F) Gains and phases in VVOR.

(G) Training sessions for motor learning (cartoons) consisted of in-phase rotation of the vestibular and visual input with the same amplitude (5°, 0.6 Hz) on the first training day and increasing amplitude of visual input afterward. This training induced a reversal of VOR phase. Gray dots indicate individual data points. See Table S1 for statistics. *$p < 0.05$, ***$p < 0.001$.

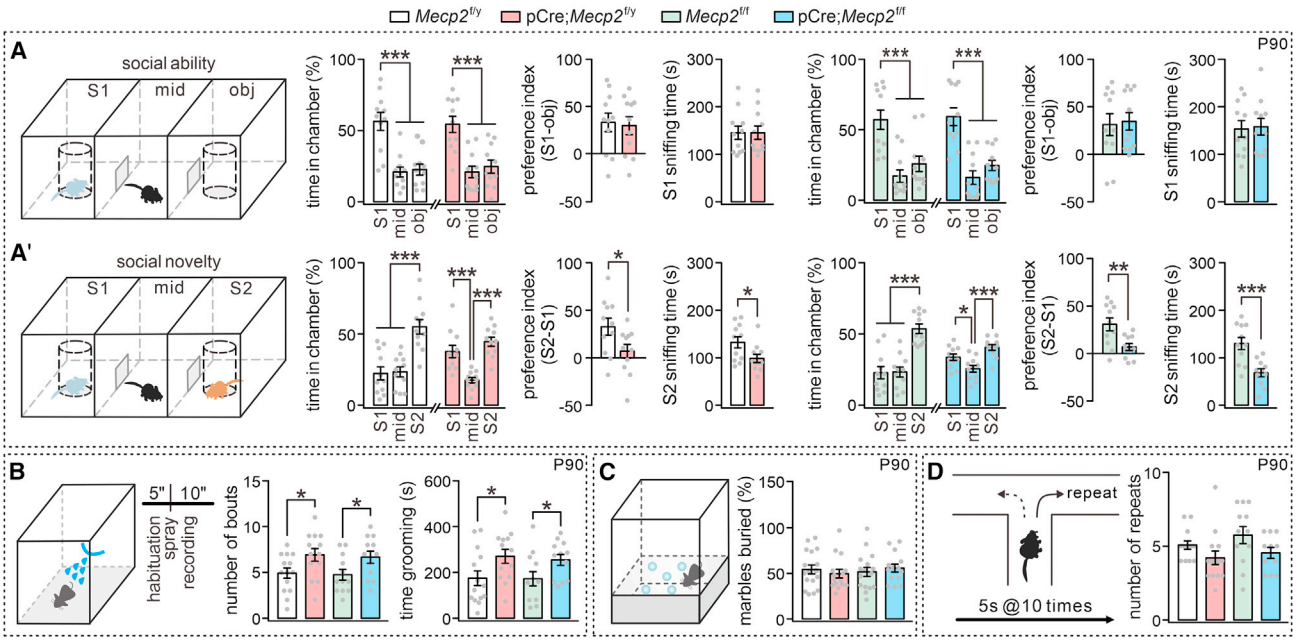


**Figure 2. Social impairment and repetitive behaviors in cKO mice (P90)**

(A) Social ability evaluated by time spent in each chamber and sniffing time (n = 11 for each group). Bar graphs: time spent in S1, middle (mid), and object (obj) chambers and sniffing time of control and cKO mice at P90.

(A′) Social novelty test following the introduction of S2.

(B) Cumulative time spent and number of bouts engaged in water spray-induced grooming behavior were scored over a 10-min session ($Mecp2^{f/y}$, n = 14; pCre:$Mecp2^{f/y}$, n = 13; $Mecp2^{f/f}$, n = 12; pCre:$Mecp2^{f/f}$, n = 12).

(C) No difference between cKO mice and controls in the marble-burying task ($Mecp2^{f/y}$, n = 17; pCre:$Mecp2^{f/y}$, n = 15; $Mecp2^{f/f}$, n = 16; pCre:$Mecp2^{f/f}$, n = 14).

(D) No difference between cKO mice and controls in the T maze paradigm ($Mecp2^{f/y}$, n = 13; pCre:$Mecp2^{f/y}$, n = 14; $Mecp2^{f/f}$, n = 12; pCre:$Mecp2^{f/f}$, n = 11). See Table S2 for statistics. *p < 0.05, **p < 0.01, ***p < 0.001.

both control and cKO mice (Figure S4E), suggesting that CF elimination develops normally in cKO mice.

PCs also receive inhibitory inputs from interneurons (Figure S4A). Thus, we measured miniature and evoked inhibitory postsynaptic currents (mIPSCs and eIPSCs, respectively). Neither the frequency nor amplitude of mIPSCs was affected by *Mecp2* deletion (Figure S4F). Mean eIPSC amplitudes at various stimulation intensities were comparable between two groups (Figure S4G). These recordings suggest that GABAergic transmission onto PCs is not affected by *Mecp2* deletion. To examine the excitatory-inhibitory input ratio in PCs, constant stimulation was applied to PFs, and eIPSCs or eEPSCs were recorded sequentially from the same PC. No difference in excitatory-inhibitory input ratio was found between control and cKO PCs (Figure S4H).

In addition, we examined whether metabotropic glutamate receptor 1 (mGluR1) is affected in cKO mice. Western blots showed that synaptic expression of mGluR1, GluA2, and excitatory amino acid exchanger 4 (EAAT4) was unaltered in cKO mice (Figure S4I). We found that the peak amplitude of mGluR1-EPSCs was comparable between control and cKO mice (Figure S4J), suggesting that mGluR1 is not affected by PC deletion of *Mecp2*.

## Reduced intrinsic excitability in late adolescent cKO mice

What is the mechanism causing abnormal behaviors of cKO mice? Intrinsic excitability may be a candidate because it is altered in mouse models of ASD and Rett syndrome.[7,10,22,28] Moreover, PC excitability is critical for the output of the cerebellar cortex, which further regulates cerebello-cerebral loops that give rise to the profile of psychiatric deficits.[6] Hence, we examined intrinsic excitability of PCs in mice at P30. Action potentials (APs) of PCs, referred to as simple spikes *in vivo*,[29] were recorded following a rheobase current (Figure 3A). AP parameters, including threshold, amplitude, half-width, and afterhyperpolarization potential (AHP), were measured (Figure 3B). We found that control and cKO PCs had a similar AP pattern (Figure 3C). In addition, APs of control and cKO PCs showed a comparable threshold, amplitude, half-width and AHP (Figure 3D). Intrinsic excitability was assessed by injecting stepped currents of increasing amplitude on PCs. Our results showed a linear current-to-firing frequency relationship with similar slopes in both groups (Figure 3E). These findings indicate that PC intrinsic excitability is normal in cKO mice at P30.

The examination of the excitability of PCs acquired different results at P90. First, AHP amplitude increased in cKO PCs (Figures 3F and 3G). Second, current injection evoked fewer spikes in cKO PCs compared with control PCs (Figure 3H), demonstrating that PC excitability is reduced in cKO mice at P90. Next, we investigated whether synaptic transmission is affected by MeCP2 deficit at P90. In summary, our results argue against this possibility. First, neither the frequency nor amplitude of mEPSCs was altered in cKO mice (Figure S5A). Second,

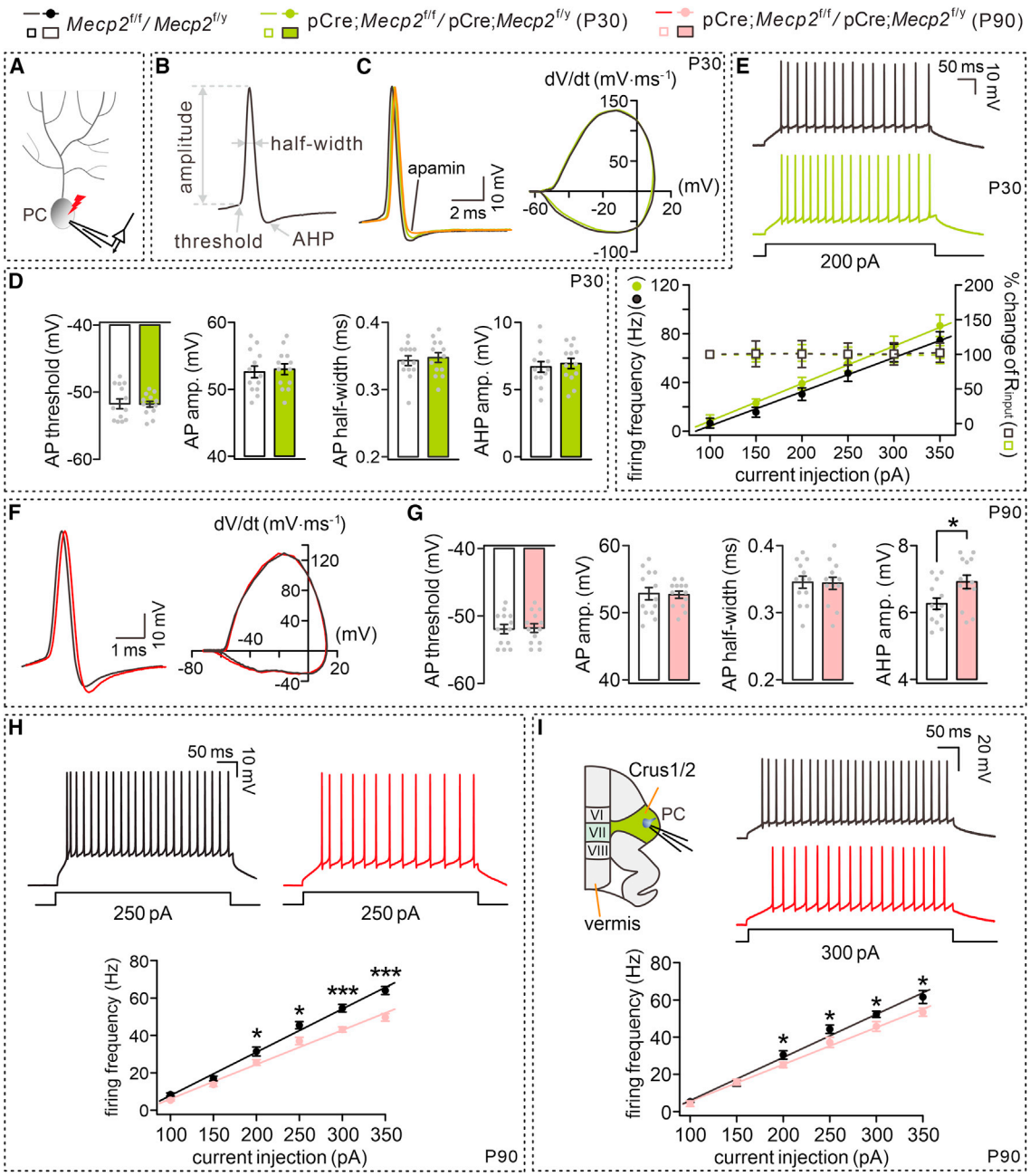


**Figure 3. Reduced intrinsic excitability of PCs in adolescent cKO mice**

(A) A diagram of whole-cell recording with current injection in PCs from the cerebellar vermis, which is applicable to the experiments shown in (B)–(H).

(B) Representative APs obtained by injecting a depolarizing current (50 ms; range 0.1–0.3 nA) in PCs. Arrowheads indicate the measurement of threshold, amplitude, half-width, and AHP.

(C) Representative APs induced by a depolarizing current in control and cKO mice (P30). Note that AHP was blocked by apamin (100 nM), a specific inhibitor of SK2 (n = 5). Right: phase-plane plots ($V_m$ vs. dV/dt) ($V_m$, membrane potential; dV, delta change of voltage; dt, delta change of time) for APs on the left.

(D) No difference was found in threshold, amplitude, half-width, or AHP between control and cKO mice (P30) (n = 20 for each group).

(E) Example traces of current pulse-evoked spikes of PCs from control and cKO mice (P30) in response to a 200-ms/200-pA current injection. Bottom: input-output curves for injected currents and firing frequency. Input resistance ($R_{input}$) was monitored during the course of the experiment, and the percentages of changes are shown after normalization to the first point.

(F) Representative APs of PCs in mice (P90). Right: phase-plane plots for APs.

(G) Averages of threshold, amplitude, half-width, and AHP (control, n = 13; cKO, n = 11).

*(legend continued on next page)*

neither the amplitude nor PPF of PF-EPSCs was different between control and cKO mice (Figure S5B). Third, no difference in the amplitude or PPD of CF-EPSCs was found between control and cKO mice (Figure S5C). Fourth, all CF-EPSCs were elicited in an all-or-none fashion in both control and cKO mice (Figure S5D). Fifth, neither the frequency nor amplitude of mIPSCs was affected by *Mecp2* deletion (Figure S5E). Finally, mean eIPSCs in response to different stimulation intensities were comparable between control and cKO groups (Figure S5F).

Previous work has shown that the inhibition of PC activity in the Crus1/2 area generates ASD-related behaviors.[11] Thus, we investigated whether *Mecp2* deletion affects the excitability of Crus PCs at P90. Indeed, Crus1/2 PCs in cKO mice fired fewer spikes as well (Figure 3I), indicating that *Mecp2* deletion reduces the excitability of Crus1/2 PCs. As a control, we also examined APs and intrinsic excitability of Crus1/2 PCs at P30. Our results showed that AP parameters, including threshold, amplitude, half-width, and AHP, were not affected by MeCP2 deficit in these PCs at this stage (Figure S6A), which is in line with the results obtained from vermal PCs (Figure 3D). We also injected current steps in Crus 1/2 PCs at P30 and examined their intrinsic excitability. Our results indicated similar linear current-to-firing frequency relationships between control and cKO Crus1/2 PCs (Figure S6B). These findings indicate that Crus1/2 cKO PCs also have normal intrinsic excitability at P30.

## Small-conductance calcium-activated $K^+$ (SK) channels are upregulated in cKO mice

Next, we investigated which molecular event might influence PC excitability. We focused on SK channels because both pharmacological blockade of SK and deletion of *Kcnn2*, the gene that encodes SK2, can enhance PC excitability.[24] Total and surface expression of SK2 was unchanged in cKO mice at P30 (Figure 4A), but surface SK2 was increased significantly in cKO mice at P90 (Figure 4A). Furthermore, we found that SK2 currents obtained at each holding potential were larger in cKO PCs than those in control PCs, which was also shown by the current-voltage (I-V) relationship plots (Figure 4B). In addition, we found that *Mecp2* deletion did not affect SK2 currents at P30, as shown by an unchanged I-V relationship (Figure 4B).

We recorded SK2-mediated tail currents,[30–32] which are elicited by a transient $Ca^{2+}$ influx responding to a depolarizing voltage step and shown as a resurgent current immediately after returning to the holding voltage.[30] For a series of voltage steps from −40 to +30 mV before jumping back to a holding current of −50 mV, SK2-mediated tail currents were markedly larger in cKO PCs at potentials more positive than −20 mV (Figure 4C). Moreover, tail currents were recorded in Crus1/2 PCs, and they were also augmented (Figure 4D). Collectively, our results suggest that *Mecp2* deletion enhances SK2 currents.

In addition, we asked whether *Mecp2* deletion affects hyperpolarization-activated cyclic nucleotide-gated 1 (HCN1) and HCN2 channels, the major isoforms of the HCN family in PCs[33] that contribute to the hyperpolarization-activated current ($I_h$) and regulate motor learning.[34] Our results indicated that neither HCN1 and HCN2 expression nor $I_h$ was affected by PC deletion of *Mecp2* (Figure S7).

## MeCP2 regulates SK2 through BDNF-TrkB signaling and PTP1B

We continued to investigate the underlying molecular events that link *Mecp2* deletion to SK2 up-regulation. Among a large number of molecular signatures driven by *Mecp2* mutation, BDNF and its receptor, tyrosine kinase receptor B (TrkB), are regulated by *Mecp2*.[35,36] Moreover, BDNF signaling is considered one of therapeutic targets for treating Rett syndrome.[37] Inspired by these findings, we asked whether BDNF signaling participates in the regulation of SK2 by *Mecp2* deletion. BDNF (50 ng/mL) was applied to cerebellar slices of control mice for 30 min, and SK2 and TrkB were evaluated immediately. Administering BDNF enhanced the tyrosine phosphorylation of TrkB at 706, and it also significantly decreased surface SK2 (Figure 5A). Subsequently, SK2 currents were recorded in control or BDNF-containing solution, and they were reduced by BDNF application. These results show that BDNF/TrkB signaling negatively regulates SK2 (Figure 5B).

A parallel question was whether *Mecp2* deletion affects the phosphorylation of TrkB. We measured the tyrosine phosphorylation of TrkB-Y706, which is essential for the activity of TrkB.[38] Interestingly, western blots revealed an age-dependent action of *Mecp2* deletion; the phosphorylation of TrkB-Y706 was intact at P30 but inhibited at P90 (Figure 5C). Meanwhile, total TrkB was unaffected at both ages (Figure 5C). These results suggest that *Mecp2* deletion reduces TrkB activity and downregulates surface SK2. The effect of BDNF was verified by recording SK2 currents in cKO slices. Our results showed that SK currents decreased with BDNF application (Figure 5D), and the attenuation of SK currents was more pronounced in cKO mice (Figures 5B and 5D), suggesting that BDNF-TrkB signaling and MeCP2 work through same pathway to control SK2 expression.

However, the question remained how *Mecp2* deletion regulates the phosphorylation of TrkB in an age-dependent manner. It has been reported that the expression of PTP1B, a protein tyrosine phosphatase, increases due to *Mecp2* disruption and that this increase is sufficient to downregulate tyrosine phosphorylation of TrkB.[39] Likewise, we found that there was a development-dependent regulation of *Mecp2* on PTP1B expression; PTP1B was unchanged in cKO mice at P30 but increased at P90 (Figure 5E). Furthermore, a series of experiments was conducted to confirm the roles of PTP1B on TrkB signaling and PC excitability. First, an antagonist of PTP1B,[39,40] CPT-157633 (1 μM), was applied to cerebellar slices (P90) of cKO mice for 30 min, and the phosphorylation of TrkB was evaluated. We found that the application of CPT-157633 significantly increased the phosphorylation level of

(H) Example traces of current pulse (250 ms/250 pA)-induced spontaneous spikes of PCs. Bottom: input-output curves for injected currents and firing frequency. For the imitation, $y_0$ values were −15.3 (control) and −12.2 (cKO); slope (*a*) values were 0.23 (control) and 0.18 (cKO) (control, n = 13; cKO, n = 12).
(I) Schematic showing whole-cell recording of PCs in Crus1/2 of mice (P90). Right: example traces from Crus1/2 PCs in response to a 300-ms current injection. Bottom: input-output curves for injected currents and firing frequency. For the imitation, $y_0$ values were −17.3 (control) and −14.4 (cKO); slope (*a*) values were 0.23 (control) and 0.20 (cKO) (n = 10 for each group). Gray dots indicate individual data points. See Table S3 for statistics. *p < 0.05, ***p < 0.001.

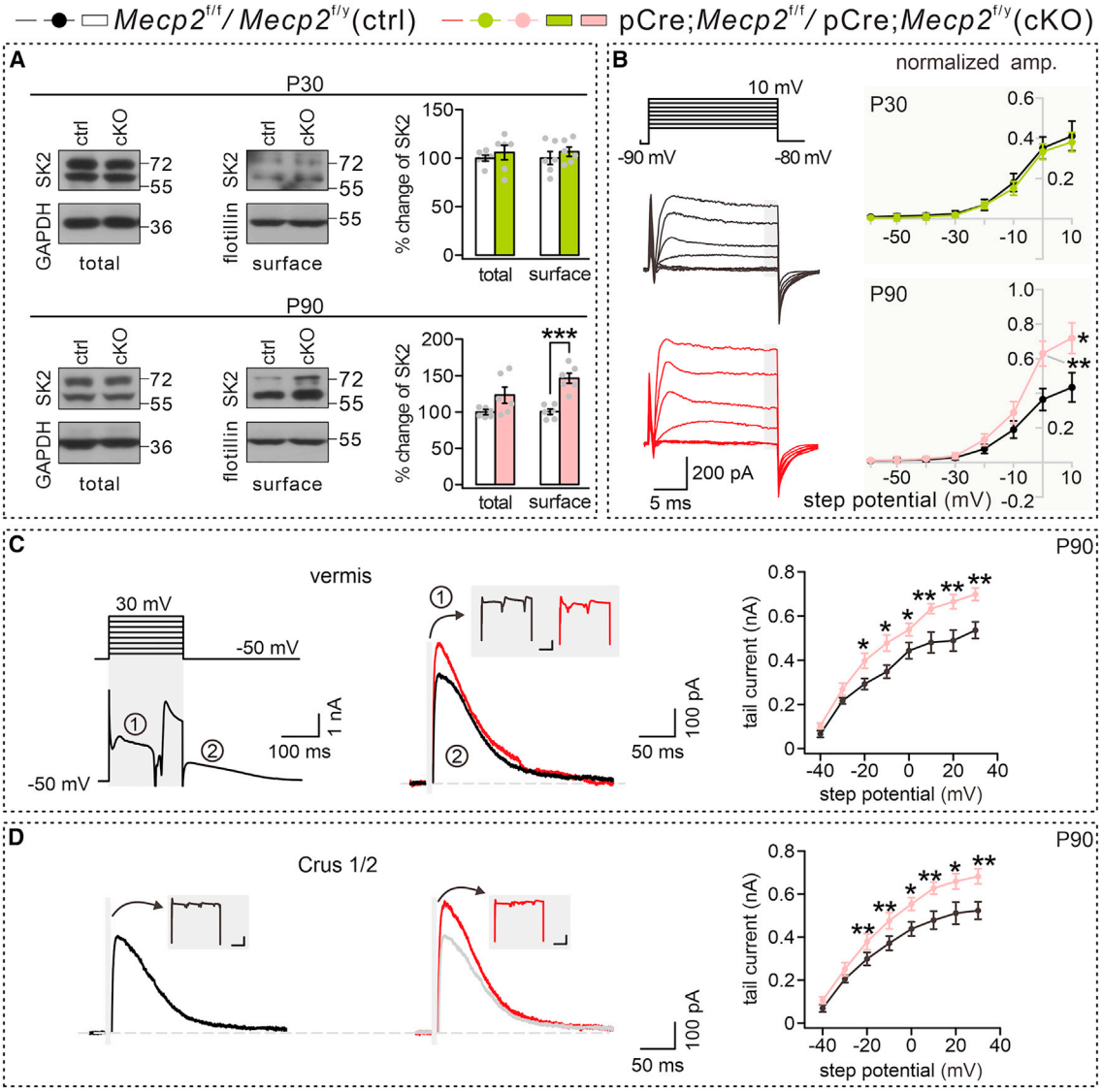


**Figure 4. Increased SK2 currents in adolescent cKO mice**

(A) Total and surface SK2 in the cerebellum. Glyceraldehyde-3-phosphate dehydrogenase (GAPDH) and flotillin were internal controls of total and surface protein, respectively. Histograms show percentage changes of SK2 in cKO mice relative to control.

(B) Left: representative SK2 currents induced by voltage steps in control (black) and cKO (red) mice at P90. Right: current-voltage (I-V) curves derived from P30 and P90 mice, with current amplitudes normalized to the maximal value. Recording site: cerebellar vermis. P30: control, n = 8; cKO, n = 7. P90: control, n = 9; cKO, n = 8.

(C) Left: stimulation paradigm and a representative current trace with two regions, where #1 represents an inward $Ca^{2+}$ current complex, and #2 represents an outward tail current. Center: representative tail currents evoked by the step to −30 mV. Scale bars in the inset, 50 ms/100 pA. Right: peak tail currents were plotted against step potentials. Recording site: cerebellar vermis. Control, n = 9; cKO, n = 8.

(D) Tail currents evoked by the step to −30 mV in Crus1/2 PCs from control (black) and cKO (red) mice (P90). They gray trace is the copy of control for comparison. Scale bars in the inset, 50 ms/100 pA. Right: I-V relationship of tail currents. Gray dots indicate individual data points. Recording site: cerebellar vermis. n = 9 for each group. See Table S4 for statistics. *p < 0.05, **p < 0.01, ***p < 0.001.

TrkB-Y706 in control slices without changing total TrkB (Figure S8A). Furthermore, CPT-157633 also reversed the phosphorylation of TrkB-Y706 in cKO slices, approximating it to a similar level to PTP1B inhibition on control slices (Figure S8A). Second, we examined the effect of CPT-157633 on APs of control and cKO PCs (P90) by measuring threshold, amplitude, half-width, and AHP. Our results showed that CPT-157633 did not alter the threshold, amplitude, or half-width in control or cKO PCs but reduced AHP in both control and cKO PCs (Figure S8B). Third, intrinsic excitability was assessed by injecting stepped currents on control and cKO PCs (P90) with or without CPT-157633. We found that CPT-157633 increased PC excitability in both control

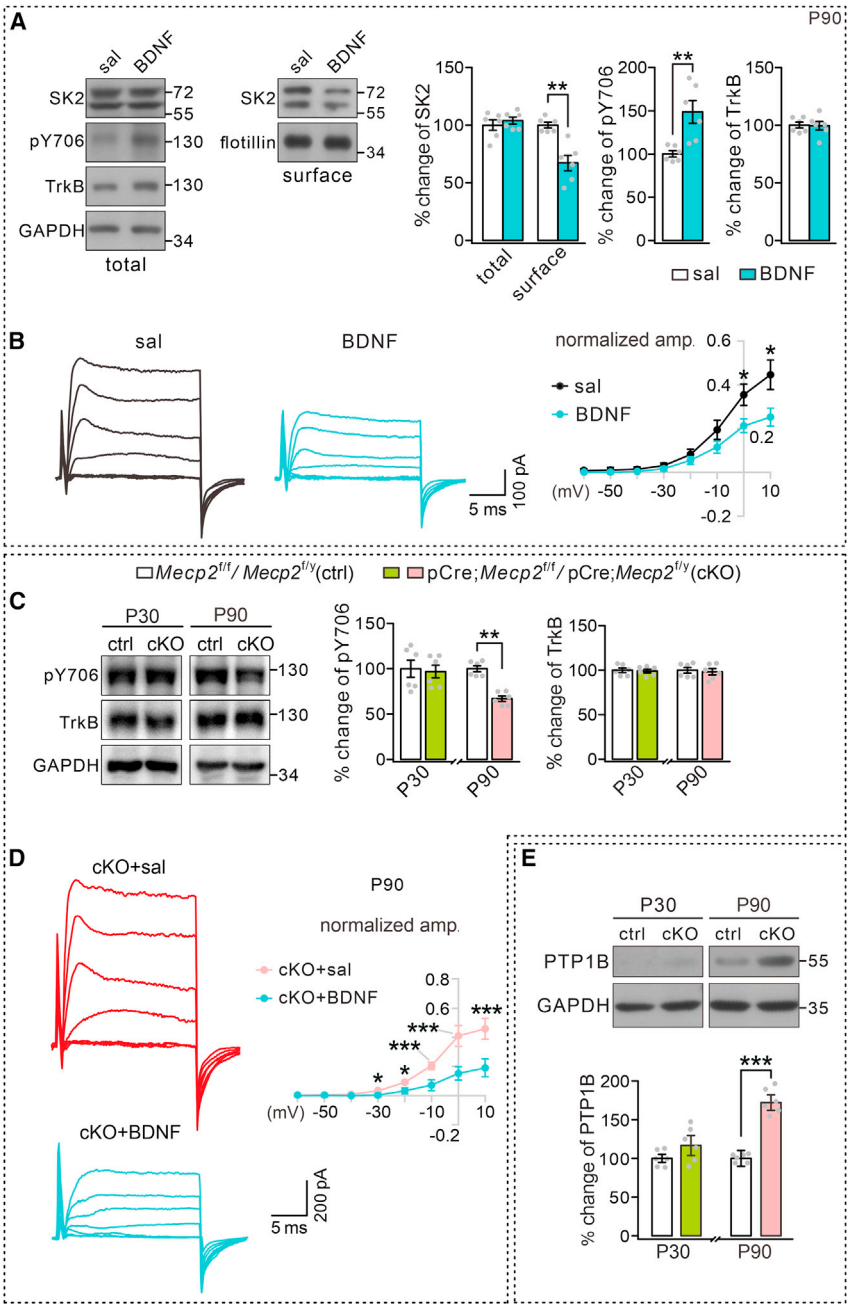


**Figure 5. Effect of BDNF-TrkB signaling on SK2**

(A) Surface SK2, phosphorylated TrkB$^{Y706}$ (pY706), and total TrkB in the cerebellum of WT mice (P90) treated with saline (sal) or BDNF. GAPDH and flotillin were internal controls. n = 6 for each group.

(B) Left: representative SK2 currents recorded from PCs treated with sal and BDNF, respectively. Right: I-V curves of sal- and BDNF-treated PCs. Recording site: cerebellar vermis. Control+sal: n = 8; cKO+sal: n = 7.

(C) Phosphorylated TrkB$^{Y706}$ and total TrkB in the cerebellum. n = 6 for each group.

(D) Left: representative SK2 currents from cKO PCs treated with sal and BDNF. Right: I-V curves. Current amplitudes were normalized to the maximal value; thus, the y axis indicates normalized currents. Recording site: cerebellar vermis. n = 7 for each group.

(E) PTP1B expression in the cerebellum. Gray dots indicate individual data points. n = 6 for each group. See Table S5 for statistics. *p < 0.05, **p < 0.01, ***p < 0.001.

## TrkB$^{Y706E}$ expression in PCs recovers SK currents and intrinsic excitability in pCre;*Mecp2*$^{f/y}$ mice

Given that *Mecp2* controls TrkB and SK2, a critical question was whether rescuing the TrkB level was enough to recover SK2 upregulation caused by *Mecp2* deletion. Confirming this hypothesis would strengthen the causal link from TrkB to SK2. To address this question, an adeno-associated virus serotype 9 (AAV9)-based double-floxed inverse orientation (DIO)-GFP-TrkB-Y706E-FLAG (TrkB$^{Y706E}$) vector was constructed, and an AAV9-based GFP vector acted as the naive control (NC) (Figure 6A), because TrkB-Y706E increases the phosphorylation and activity of TrkB.[38] The virus was injected into the middle cerebellar lobules of pCre;-*Mecp2*$^{f/y}$ mice (P30). TrkB$^{Y706E}$ was expressed in PCs due to the presence of Cre, shown by a GFP signal abundantly expressed in PCs (Figure 6A). Viral expression was also confirmed by expression of the FLAG tag (Figure 6B). Moreover, both total TrkB and TrkB$^{Y706E}$ were elevated after injection with GFP-TrkB$^{Y706E}$ (Figure 6C), indicating the efficiency of viral infection.

SK2 expression and currents were examined in PCs transduced with NC and TrkB$^{Y706E}$ vectors. TrkB$^{Y706E}$ expression significantly decreased surface SK2 without affecting total expression (Figure 6D). SK2 currents were reduced in PCs transduced with GFP-TrkB$^{Y706E}$ compared with NC (Figures 7A and 7B). Moreover, SK2-mediated tail currents markedly decreased in TrkB$^{Y706E}$-transduced cells compared with NC (Figure 7C). Collectively, these results indicate that Y706E expression attenuates SK2 currents in cKO PCs.

and cKO PCs (Figure S8C). Finally, SK2 currents were recorded in control PCs and cKO PCs with or without CPT-157633. The I-V curves demonstrate that inhibiting PTP1B could reduce SK2 currents under the conditions of both control and MeCP2 deficit (Figure S8D).

Taken together, our results reveal unrecognized PTP1B-TrkB-SK2 signaling in PCs that is independent of MeCP2 deficit. Through this mechanism, PC deletion of *Mecp2* can cause a late adolescent elevation in PTP1B expression, which further down-regulates TrkB phosphorylation and enhances membrane expression of SK2.

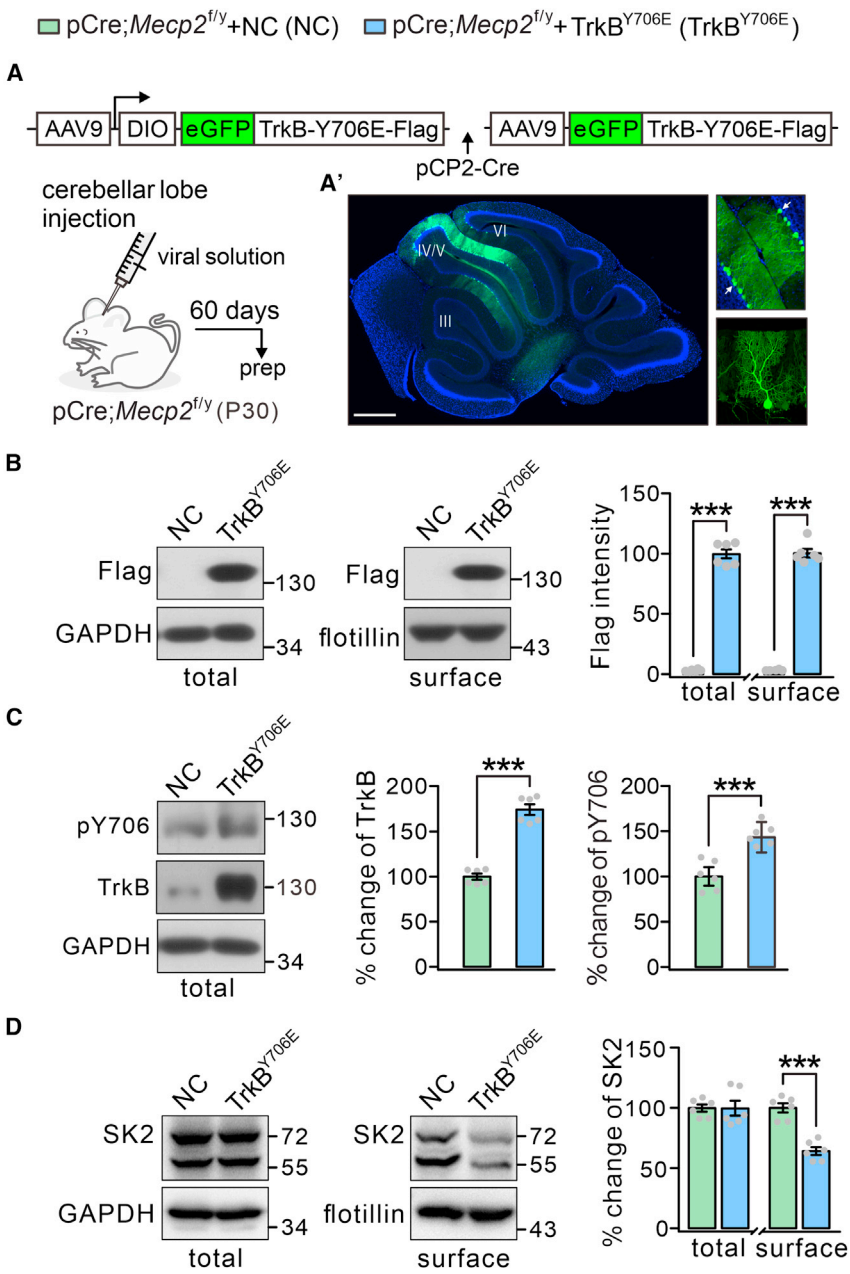


**Figure 6. Viral expression of TrkB$^{Y706E}$ in pCre;*Mecp2*$^{f/y}$ mice**

(A) Schematic of the AAV9 vector encoding EGFP-TrkB-Y706E-FLAG driven by the synapsin promoter and induced by DIO with pCP2-Cre recombinase. Bottom: anatomical targeting with stereotactic viral infusion.

(A′) Sagittal section of the cerebellum (scale bar, 500 μm) containing EGFP-labeled PCs.

(B) FLAG expression in pCre;*Mecp2*$^{f/y}$ mice treated with AAV9-EGFP (NC, n = 5) or AAV9-EGFP-TrkB-Y706E-FLAG (TrkB$^{Y706E}$, n = 5). GAPDH and flotillin were internal controls.

(C) Phosphorylated TrkB$^{Y706}$ (pY706) and total TrkB in pCre;*Mecp2*$^{f/y}$ mice treated with AAV9-EGFP or AAV9-EGFP-TrkB-Y706E-FLAG. n = 6 for each group.

(D) Total and surface SK2 in pCre;*Mecp2*$^{f/y}$ mice treated with AAV9-EGFP or AAV9-EGFP-TrkB-Y706E-FLAG. n = 6 for each group. Gray dots indicate individual data points. See Table S6 for statistics. ***p < 0.001.

Finally, APs and intrinsic excitability of cKO PCs were examined. TrkB$^{Y706E}$ expression did not change thresholds but significantly decreased AHP of cKO PCs (Figure 7D), making it similar to control levels (control, 6.1 ± 0.2 mV; TrkB$^{Y706E}$, 5.9 ± 0.3 mV; p = 0.26). Current injection evoked more spikes in TrkB$^{Y706E}$ cKO PCs than NC PCs, and the plot of firing frequency vs. injected current showed that TrkB$^{Y706E}$ cKO PCs were more excitable than NC (Figure 7E). Moreover, PC excitability was compared between control PCs and PCs receiving TrkB$^{Y706E}$ infection. Again, TrkB$^{Y706E}$ significantly decreased AHP (Figure S9A). Current injection evoked more spikes in TrkB$^{Y706E}$-expressing control PCs than NC PCs (Figure S9B). Taken together, transducing phosphorylated TrkB can reduce SK2 currents and increase excitability in either control PCs or PCs with *Mecp2* deletion.

## TrkB$^{Y706E}$ expression in PCs rescues motor and non-motor behaviors

Given the results above, we asked whether transducing TrkB$^{Y706E}$ could rescue impaired behaviors of pCre;*Mecp2*$^{f/y}$ mice. To this end, we injected AAV9 containing GFP-tagged TrkB$^{Y706E}$ or GFP vehicle into contiguous vermal lobules, the flocculus, and Crus1/2 of pCre;*Mecp2*$^{f/y}$ mice at P30 and performed behavioral tests 2 months later.

First, we examined locomotion after NC and TrkB$^{Y706E}$ expression in the middle lobules of the vermal cerebellum and the flocculus (Figures S10A and S10B). Compared with NC, TrkB$^{Y706E}$-treated cKO mice exhibited longer latency to fall from the rotarod after 5 sessions (Figure 7F). In the compensatory eye movement test, TrkB$^{Y706E}$ did not change the gain or phase of the OKR (Figure S11A), VOR (Figure S11B), or VVOR (Figure S11C). During the phase-reversal VOR adaptation test, NC or TrkB$^{Y706E}$-treated pCre;*Mecp2*$^{f/y}$ mice exhibited a similar increase in VOR gain on all days (Figure 7G). However, TrkB$^{Y706E}$-transduced mice displayed a significant increase in VOR phase compared with NC mice (day 4, p < 0.001; day 5, p < 0.001; ANOVA repeated measures) (Figure 7G). These results reveal that TrkB$^{Y706E}$ expression is sufficient to rescue the impaired motor learning of pCre;*Mecp2*$^{f/y}$ mice.

Second, we evaluated whether TrkB$^{Y706E}$ expression in PCs of lobules IV, V, and VI and Crus1/2 could rescue autistic-like behaviors in pCre;*Mecp2*$^{f/y}$ mice (Figure S10C). In the social approach

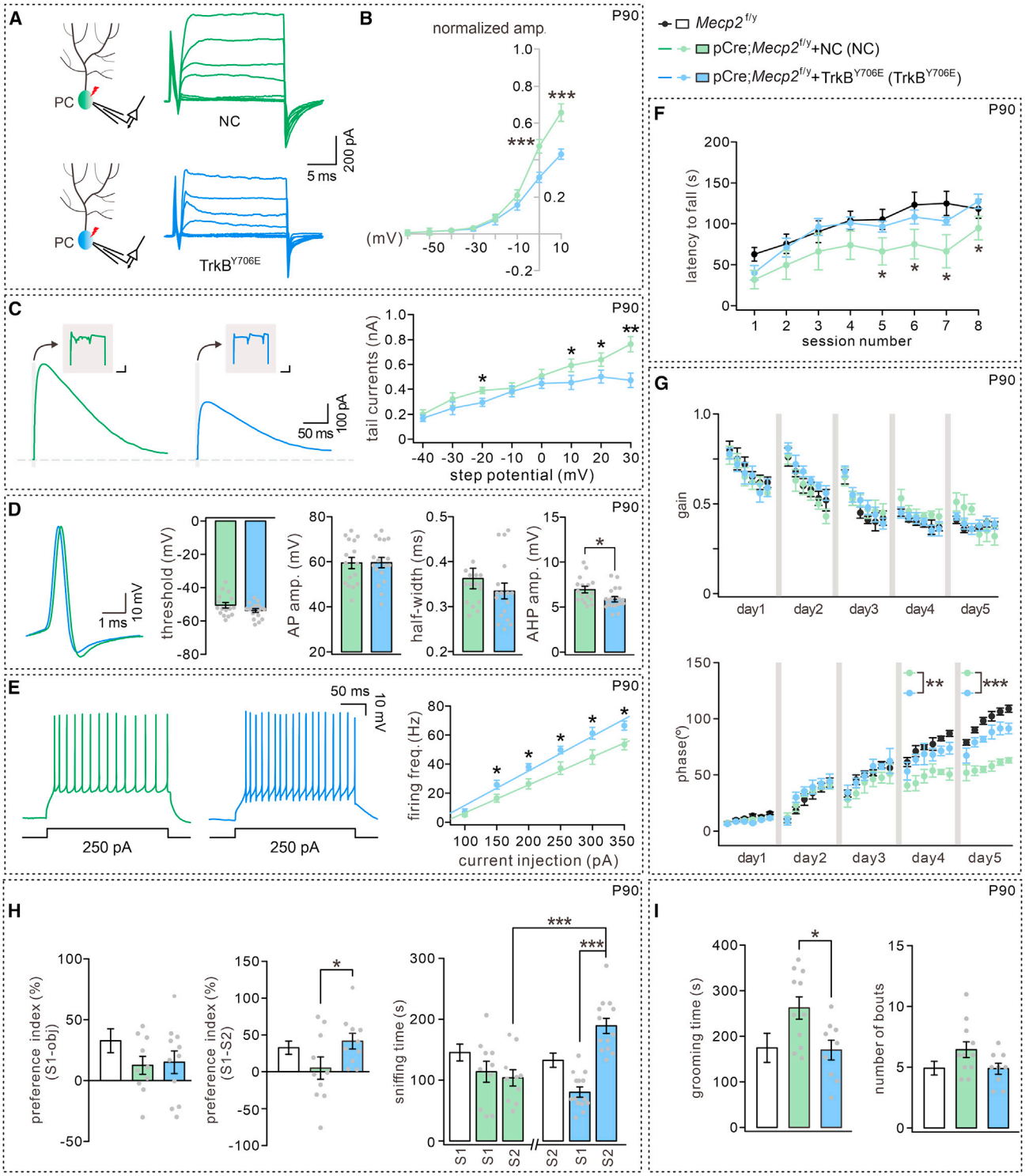


**Figure 7. PC Excitability and impaired behaviors are rescued by TrkB$^{Y706E}$ in pCre;*Mecp2*$^{f/y}$ PCs**

(A) Green and blue traces show representative SK2 currents from pCre;*Mecp2*$^{f/y}$ PCs treated with AAV9-EGFP (NC) or AAV9-EGFP-TrkB-Y706E-FLAG (TrkB$^{Y706E}$), respectively. Recording site: cerebellar vermis.

(B) I-V curves of NC and TrkB$^{Y706E}$ PCs. Current amplitudes were normalized to the maximal value; thus, the y axis indicates normalized currents. 0 mV: 0.48 ± 0.04 (NC, n = 7) and 0.31 ± 0.03 (TrkB$^{Y706E}$, n = 6), p = 0.0025. 10 mV: 0.66 ± 0.05 (NC, n = 7) and 0.43 ± 0.03 (TrkB$^{Y706E}$, n = 6), p = 0.0024. Unpaired t test.

*(legend continued on next page)*

test, the mice transduced with NC and TrkB$^{Y706E}$ vectors did not differ in the preference to S1 (Figure 7H). In the social novelty test, GFP-transduced pCre;*Mecp2*$^{f/y}$ mice demonstrated impaired social interaction similar to untreated pCre;*Mecp2*$^{f/y}$ mice, as shown by low preference to S2 and short sniffing time to S2 (Figure 7H). Interestingly, introducing TrkB$^{Y706E}$ in cKO PCs recovered the response of the mouse to social novelty, as shown by increased preference and sniffing time to S2 (Figure 7H). These findings were further corroborated by the resident-intruder test, in which TrkB$^{Y706E}$ expression successfully rescued the social memory defect of cKO mice, when they interacted with the familiar mice (Figures S2E and S2F). We further evaluated whether TrkB$^{Y706E}$ expression in PCs impacts repetitive behaviors and open field performance of pCre;*Mecp2*$^{f/y}$ mice. We found that TrkB$^{Y706E}$ expression ameliorated grooming time, though the number of grooming bouts was unaltered (Figure 7I). Taken together, our results suggest that the introduction of TrkB in PCs might ameliorate part of the autistic-like behaviors in pCre;*Mecp2*$^{f/y}$ mice.

## DISCUSSION

In the present work, we show that (1) PC deletion of *Mecp2* impairs motor learning and causes autistic-like behaviors, (2) *Mecp2* deletion in PCs does not change glutamatergic or GABAergic transmission and instead promotes surface expression and currents of SK2 channels and affects the intrinsic excitability, (3) *Mecp2* deletion gradually increases PTP1B and ultimately attenuates TrkB activity, (4) BDNF/TrkB signaling regulates the surface expression of SK2, and (5) the expression of TrkB$^{Y706E}$ in adult *Mecp2*-null PCs is sufficient to restore PC function and rescue both motor and non-motor behavioral deficits. In short, we show a MeCP2 signaling pathway that controls PC excitability by regulating TrkB activity through PTP1B. Accordingly, MeCP2 deficiency augments SK2 currents, reduces intrinsic excitability, and distorts motor and non-motor behaviors. Previous work claims that *Mecp2* deletion from the cerebellum, hindbrain, and/or spinal cord causes limited motor deficits.[23] Here we expanded on that work through more in-depth experiments and analyses and revealed that MeCP2 in PCs is indeed relevant to a variety of motor and non-motor behaviors.

### Distinct functions of MeCP2 in neurons

MeCP2 is widely expressed in neurons and glial cells and regulates their development and function.[41] In the cerebral cortex, MeCP2 regulates the strength of excitatory synaptic transmission of pyramidal cells,[42] while its loss in inhibitory neurons reduces GABAergic transmission.[22] Here, we show that MeCP2 in PCs affects surface SK2 and intrinsic excitability rather than EPSCs and IPSCs. It is a long-standing question to what extent loss of MeCP2 is involved in neurogenesis and synaptic development.[43] Hippocampal pyramidal cells of Rett syndrome mouse models exhibit reductions in neuronal soma size, dendritic arborization, spine density, PSD95 expression, and synaptic scaling.[44–46] While these findings show the participation of MeCP2 in neuronal maturation, our work indicates that MeCP2 does not exert an effect on the development of PCs. Thus, MeCP2 may have different molecular actions in different cell types. These heterogeneous effects are in line with the great variety in the methylation landscape across cell types in *Mecp2*$^{T158\ M/y}$ and *Mecp2*$^{R106\ W/y}$ mice.[47]

### MeCP2 activity, BDNF-TrkB signaling, and SK2

MeCP2 not only represses[48,49] but also promotes[50,51] the expression of BDNF, depending on its phosphorylation status.[52] In fact, MeCP2 has versatile roles in transcription, microRNA expression, and RNA splicing[35,41] and dually regulates gene expression by combining repressor and activator effects.[53,54] The present work links BDNF/TrkB signaling with upstream PTP1B and downstream SK2, strengthening the notion that BDNF/TrkB signaling is an essential effector of MeCP2 in Rett syndrome. While our result showing that $I_h$ is not affected by *Mecp2* deletion strengthens the notion that SK2 is the target of TrkB, it cannot be excluded that other channels are also involved in TrkB signaling with *Mecp2* deletion. Our data align well with the study by Krishnan et al.[39] demonstrating that disruption of MeCP2 function increases PTP1B levels and thereby decreases the tyrosine phosphorylation of TrkB. Moreover, our observation that increasing TrkB activity is sufficient to rescue PC dysfunction raises a possibility to design therapies for Rett syndrome. A previous study has shown that protein kinase A can regulate surface SK2 through direct phosphorylation.[55] Thus, it is possible that TrkB regulates the phosphorylation sites of SK2, leading to the reorganization of SK2 surface expression in response to the condition of either reduced TrkB or TrkB-Y706E expression.

### ASD genes and their impacts on cerebellar physiology

More than 1,000 risk genes have been found for ASD, and the number of genes with *de novo* mutations is still growing. While

(C) Tail currents evoked by voltage step to −30 mV in pCre;*Mecp2*$^{f/y}$ PCs treated with AAV9-EGFP (n = 12) or AAV9-EGFP-TrkB-Y706E-FLAG (n = 10), respectively. Scale bars in the inset, 50 ms/100 pA. Recording site: cerebellar vermis.

(D) Representative APs of PCs in NC (n = 16) and TrkB$^{Y706E}$ (n = 17) groups. Bar graphs show the statistics of threshold, amplitude, half-width, and AHP. Recording site: cerebellar vermis.

(E) Example traces of PCs in response to a 250-ms/250-pA current injection. Right: input-output curves for injected currents and firing frequency. For the imitation, $y_0$ values were −12.8 (NC) and −12.0 (TrkB$^{Y706E}$); slope (*a*) values were 0.19 (NC) and 0.24 (TrkB$^{Y706E}$). Recording site: cerebellar vermis. NC, n = 11; TrkB$^{Y706E}$, n = 9.

(F) Time spent on the rotarod for pCre;*Mecp2*$^{f/y}$ male mice treated with AAV9-EGFP (NC, n = 6) and AAV9-EGFP-TrkB-Y706E-FLAG (TrkB$^{Y706E}$, n = 8). The black line is copied from Figure 1C, showing control data.

(G) Phase-reversal VOR adaptation test in male mice. The black points are copied from Figure 1G, showing control data.

(H) Social interaction tests in male mice evaluated by time spent in each chamber and sniffing time. The black columns are copied from Figure 2A, showing control data.

(I) Number of bouts and time spent engaged in the grooming test for male mice. The black columns are copied from Figure 2B, showing control data. Gray dots indicate individual data points. See Table S7 for statistics. *p < 0.05, **p < 0.01, ***p < 0.001.

ASD can be linked to defective development of the cerebellum, relatively many of these genes, including *Tsc1/2*, *Nlgn3*, *Fmr1*, *Pten*, and *Shank2*, cause PC dysfunction with changes in electrophysiological properties.[7,8,10,56–59] For example, PCs of $Tsc1^{PC}$ and $Pten^{PC}$ mice show a reduced excitatory/inhibitory input ratio and simple spike firing,[9,10] whereas PC deletion of *Shank2* increases inhibitory currents and inhibits intrinsic plasticity.[10] We show here that loss of MeCP2 attenuates PC firing frequency through regulating SK2. Thus, *Tsc1*, *Shank2*, and *Mecp2* may share a common role in stabilizing intrinsic excitability of PCs. Other examples corroborate the concept that altered synaptic plasticity and intrinsic excitability in PCs in general lead to aberrations in social or cognitive behavior.[60,61] Thus, altered excitability of PCs together with abnormal cerebellar development may be the key factors for autistic behaviors.

### Deterioration and rescue of cerebello-cerebral connectivity

We demonstrate that expressing $TrkB^{Y706E}$ restores the intrinsic excitability of PCs as well as behavioral phenotypes in *Mecp2* cKO mice. Similarly, re-expressing fragile X mental retardation protein (FMRP) in young adult mice with fragile X syndrome has been shown to rescue synaptic organization and visual performance.[62] However, restoring the function of a gene may not only act on the pre- and/or post-synaptic sites of dendrites and cell bodies, but in young adult mammals, it might, in principle, also rescue aberrations in the related axonal outputs, especially when the rescuing endeavor takes place close to the critical developmental period. Accordingly, it will be interesting to find out to what extent abnormalities in the cerebello-cerebral pathways in *Mecp2* cKO mice can also be rescued by overexpressing $TrkB^{Y706E}$. Indeed, such an approach might eventually offer an attractive general strategy for treating genetic disorders, in which cerebello-cerebral connectivity is impaired from early on. An interesting comparable example in this respect might be tuberous sclerosis (*Tsc1*), in which the cerebello-cerebral pathway from cerebellar Crus1 to the ventromedial thalamus and medial prefrontal cortex is also affected from early on and in which the genetic defects also lead to social deficits and repetitive behaviors.[11,63] Importantly, not only the cerebello-cerebral pathways linked to Crus1 may be subject to ASD pathogenesis but also those comprising other lobules in the anterior and median cerebellar cortex.[64,65] We therefore propose that dysfunction of PC excitability and aberrations in the development of cerebello-cerebral connectivity may both contribute to ASD and that both phenomena may have to be rescued to obtain optimal therapeutic effects.

### Limitations of the study

While our study sheds light on the underlying cellular mechanisms of PC dysfunctions caused by MeCP2 deficiency, the abnormalities in the cerebello-cerebral pathways in *Mecp2* cKO mice remain unclear. We emphasize the roles of PTP1B-TrkB-SK signaling in PC excitability as well as motor and non-motor behaviors, but the evidence linking these events needs to be further strengthened. It should be noted that this signaling may be a parallel mechanistic pathway that improves the disrupted functionality but not necessarily the mechanism driving dysfunction in *Mecp2* mutants. The use of specific and development-dependent PTP1B KO animals may reveal a more complete picture of how this signaling modulates cerebellar development and animal behaviors. In addition, our present work does not answer whether other channels are involved in TrkB signaling and how SK2 is regulated by TrkB, which remains to be uncovered using more techniques.

## STAR★METHODS

Detailed methods are provided in the online version of this paper and include the following:

- KEY RESOURCES TABLE
- RESOURCE AVAILABILITY
  - Lead contact
  - Materials availability
  - Data and code availability
- EXPERIMENTAL MODEL AND STUDY PARTICIPANT DETAILS
  - Mouse
- METHOD DETAILS
  - RT-PCR
  - Surface biotinylation
  - Western blotting
  - Immunohistochemistry
  - Nissl staining
  - Golgi staining and sholl analysis
  - Recombinant virus and *in vivo* injection
  - Electrophysiology
  - Footprint test
  - Rotarod test
  - Three chamber test
  - Grooming test
  - Marble burying test
  - T-maze test
  - Resident-intruder test
  - Olfactory habituation test
  - Compensatory eye movement
- QUANTIFICATION AND STATISTICAL ANALYSIS

## SUPPLEMENTAL INFORMATION

Supplemental information can be found online at https://doi.org/10.1016/j.celrep.2023.113559.

## ACKNOWLEDGMENTS

We thank Drs. Bo Zhang, Yan Gu, and Jia-Dong Chen for valuable comments; Dr. Zi-Long Qiu for providing $Mecp2^{f/+}$ mice; and the Core Facilities of the Zhejiang University Institute of Neuroscience for technical assistance. This work was supported by grants from the National Key Research and Developmental Program of the Ministry of Science and Technology of China (2021ZD0204000 to Y.S.), the National Natural Science Foundation of China (81625006 to Y.S., 31820103005 to Y.S., 32170976 to L.Z., 32000692 to X.-T.W., and 32100791 to F.-X.X.), the Zhejiang Province Natural Science Foundation of China (LY21C090003 to L.Z.), ERC-Stg (680235 to M.S.), the Science and Technology Program of Hangzhou Municipality (20190101A10 to W.C.), the Netherlands Organization for Scientific Research (NWO-ALW 824.02.001 to C.D.Z.), the Dutch Organization for Medical Sciences (ZonMW 91120067 to C.D.Z.), Medical Neuro-Delta (MD 01092019-31082023 to C.D.Z.), INTENSE LSH-NWO (TTW/

00798883 to C.D.Z.), the Albinism Vrienden-Fonds (NIN-KNAW), ERC-adv (GA-294775 to C.D.Z.), ERC-POC (737619 and 768914 to C.D.Z.), and the NWO-Gravitation Program (DBI2).

## AUTHOR CONTRIBUTIONS

F.-X.X., X.-T.W., L.Z., C.D.Z., and Y.S. designed the research. F.-X.X., X.-T.W., X.-Y.C., J.-Y.L., J.-W.G., and L.Z. performed the research. F.Y., W.C., and M.S. supplied reagents/analytic tools. F.-X.X., X.-T.W., L.Z., and Y.S. analyzed data. F.-X.X., X.-T.W., W.C., M.S., C.D.Z., L.Z., and Y.S. wrote the paper.

## DECLARATION OF INTERESTS

The authors declare no competing interests.

Received: October 27, 2022
Revised: October 5, 2023
Accepted: November 22, 2023
Published: December 13, 2023

## REFERENCES

1. Sathyanesan, A., Zhou, J., Scafidi, J., Heck, D.H., Sillitoe, R.V., and Gallo, V. (2019). Emerging connections between cerebellar development, behaviour and complex brain disorders. Nat. Rev. Neurosci. *20*, 298–313.
2. Fujita, H., Kodama, T., and du Lac, S. (2020). Modular output circuits of the fastigial nucleus for diverse motor and nonmotor functions of the cerebellar vermis. Elife *9*, e58613.
3. Pisano, T.J., Dhanerawala, Z.M., Kislin, M., Bakshinskaya, D., Engel, E.A., Hansen, E.J., Hoag, A.T., Lee, J., de Oude, N.L., Venkataraju, K.U., et al. (2021). Homologous organization of cerebellar pathways to sensory, motor, and associative forebrain. Cell Rep. *36*, 109721.
4. Gao, Z., Davis, C., Thomas, A.M., Economo, M.N., Abrego, A.M., Svoboda, K., De Zeeuw, C.I., and Li, N. (2018). A cortico-cerebellar loop for motor planning. Nature *563*, 113–116.
5. Carta, I., Chen, C.H., Schott, A.L., Dorizan, S., and Khodakhah, K. (2019). Cerebellar modulation of the reward circuitry and social behavior. Science *363*, eaav0581.
6. Su, L.D., Xu, F.X., Wang, X.T., Cai, X.Y., and Shen, Y. (2021). Cerebellar dysfunction, cerebro-cerebellar connectivity and autism spectrum disorders. Neuroscience (San Diego, CA, U. S.) *462*, 320–327.
7. Tsai, P.T., Hull, C., Chu, Y., Greene-Colozzi, E., Sadowski, A.R., Leech, J.M., Steinberg, J., Crawley, J.N., Regehr, W.G., and Sahin, M. (2012). Autistic-like behaviour and cerebellar dysfunction in Purkinje cell Tsc1 mutant mice. Nature *488*, 647–651.
8. Reith, R.M., McKenna, J., Wu, H., Hashmi, S.S., Cho, S.H., Dash, P.K., and Gambello, M.J. (2013). Loss of Tsc2 in Purkinje cells is associated with autistic-like behavior in a mouse model of tuberous sclerosis complex. Neurobiol. Dis. *51*, 93–103.
9. Cupolillo, D., Hoxha, E., Faralli, A., De Luca, A., Rossi, F., Tempia, F., and Carulli, D. (2016). Autistic-like traits and cerebellar dysfunction in Purkinje cell PTEN knock-out mice. Neuropsychopharmacology *41*, 1457–1466.
10. Peter, S., Ten Brinke, M.M., Stedehouder, J., Reinelt, C.M., Wu, B., Zhou, H., Zhou, K., Boele, H.J., Kushner, S.A., Lee, M.G., et al. (2016). Dysfunctional cerebellar Purkinje cells contribute to autism-like behavior in Shank2-deficient mice. Nat. Commun. *7*, 12627.
11. Stoodley, C.J., D'Mello, A.M., Ellegood, J., Jakkamsetti, V., Liu, P., Nebel, M.B., Gibson, J.M., Kelly, E., Meng, F., Cano, C.A., et al. (2017). Altered cerebellar connectivity in autism and cerebellar-mediated rescue of autism-related behaviors in mice. Nat. Neurosci. *20*, 1744–1751.
12. McAfee, S.S., Liu, Y., Sillitoe, R.V., and Heck, D.H. (2019). Cerebellar lobulus simplex and Crus I differentially represent phase and phase difference of prefrontal cortical and hippocampal oscillations. Cell Rep. *27*, 2328–2334.e3.
13. Mejias, R., Chiu, S.L., Han, M., Rose, R., Gil-Infante, A., Zhao, Y., Huganir, R.L., and Wang, T. (2019). Purkinje cell-specific Grip1/2 knockout mice show increased repetitive self-grooming and enhanced mGluR5 signaling in cerebellum. Neurobiol. Dis. *132*, 104602.
14. Amir, R.E., Van den Veyver, I.B., Wan, M., Tran, C.Q., Francke, U., and Zoghbi, H.Y. (1999). Rett syndrome is caused by mutations in X-linked MECP2, encoding methyl-CpG-binding protein 2. Nat. Genet. *23*, 185–188.
15. Vignoli, A., Fabio, R.A., La Briola, F., Giannatiempo, S., Antonietti, A., Maggiolini, S., and Canevini, M.P. (2010). Correlations between neurophysiological, behavioral, and cognitive function in Rett syndrome. Epilepsy Behav. *17*, 489–496.
16. Sandweiss, A.J., Brandt, V.L., and Zoghbi, H.Y. (2020). Advances in understanding of Rett syndrome and MECP2 duplication syndrome: prospects for future therapies. Lancet Neurol. *19*, 689–698.
17. Chen, R.Z., Akbarian, S., Tudor, M., and Jaenisch, R. (2001). Deficiency of methyl-CpG binding protein-2 in CNS neurons results in a Rett-like phenotype in mice. Nat. Genet. *27*, 327–331.
18. Gemelli, T., Berton, O., Nelson, E.D., Perrotti, L.I., Jaenisch, R., and Monteggia, L.M. (2006). Postnatal loss of methyl-CpG binding protein 2 in the forebrain is sufficient to mediate behavioral aspects of Rett syndrome in mice. Biol. Psychiatr. *59*, 468–476.
19. Fyffe, S.L., Neul, J.L., Samaco, R.C., Chao, H.T., Ben-Shachar, S., Moretti, P., McGill, B.E., Goulding, E.H., Sullivan, E., Tecott, L.H., and Zoghbi, H.Y. (2008). Deletion of Mecp2 in Sim1-expressing neurons reveals a critical role for MeCP2 in feeding behavior, aggression, and the response to stress. Neuron *59*, 947–958.
20. Adachi, M., Autry, A.E., Covington, H.E., 3rd, and Monteggia, L.M. (2009). MeCP2-mediated transcription repression in the basolateral amygdala may underlie heightened anxiety in a mouse model of Rett syndrome. J. Neurosci. *29*, 4218–4227.
21. Samaco, R.C., Mandel-Brehm, C., Chao, H.T., Ward, C.S., Fyffe-Maricich, S.L., Ren, J., Hyland, K., Thaller, C., Maricich, S.M., Humphreys, P., et al. (2009). Loss of MeCP2 in aminergic neurons causes cell-autonomous defects in neurotransmitter synthesis and specific behavioral abnormalities. Proc. Natl. Acad. Sci. USA *106*, 21966–21971.
22. Chao, H.T., Chen, H., Samaco, R.C., Xue, M., Chahrour, M., Yoo, J., Neul, J.L., Gong, S., Lu, H.C., Heintz, N., et al. (2010). Dysfunction in GABA signaling mediates autism-like stereotypies and Rett syndrome phenotypes. Nature *468*, 263–269.
23. Achilly, N.P., He, L.J., Kim, O.A., Ohmae, S., Wojaczynski, G.J., Lin, T., Sillitoe, R.V., Medina, J.F., and Zoghbi, H.Y. (2021). Deleting Mecp2 from the cerebellum rather than its neuronal subtypes causes a delay in motor learning in mice. Elife *10*, e64833.
24. Grasselli, G., Boele, H.J., Titley, H.K., Bradford, N., van Beers, L., Jay, L., Beekhof, G.C., Busch, S.E., De Zeeuw, C.I., Schonewille, M., and Hansel, C. (2020). SK2 channels in cerebellar Purkinje cells contribute to excitability modulation in motor-learning-specific memory traces. PLoS Biol. *18*, e3000596.
25. Smith, R.E.W., Avery, J.A., Wallace, G.L., Kenworthy, L., Gotts, S.J., and Martin, A. (2019). Sex differences in resting-state functional connectivity of the cerebellum in autism spectrum disorder. Front. Hum. Neurosci. *13*, 104.
26. Hitti, F.L., and Siegelbaum, S.A. (2014). The hippocampal CA2 region is essential for social memory. Nature *508*, 88–92.
27. Asaka, Y., Jugloff, D.G.M., Zhang, L., Eubanks, J.H., and Fitzsimonds, R.M. (2006). Hippocampal synaptic plasticity is impaired in the Mecp2-null mouse model of Rett syndrome. Neurobiol. Dis. *21*, 217–227.
28. Zhang, W., Peterson, M., Beyer, B., Frankel, W.N., and Zhang, Z.W. (2014). Loss of MeCP2 from forebrain excitatory neurons leads to cortical hyperexcitation and seizures. J. Neurosci. *34*, 2754–2763.

29. Arancillo, M., White, J.J., Lin, T., Stay, T.L., and Sillitoe, R.V. (2015). In vivo analysis of Purkinje cell firing properties during postnatal mouse development. J. Neurophysiol. *113*, 578–591.

30. Cingolani, L.A., Gymnopoulos, M., Boccaccio, A., Stocker, M., and Pedarzani, P. (2002). Developmental regulation of small-conductance $Ca^{2+}$-activated $K^+$ channel expression and function in rat Purkinje neurons. J. Neurosci. *22*, 4456–4467.

31. Bond, C.T., Herson, P.S., Strassmaier, T., Hammond, R., Stackman, R., Maylie, J., and Adelman, J.P. (2004). Small conductance $Ca^{2+}$-activated $K^+$ channel knock-out mice reveal the identity of calcium-dependent afterhyperpolarization currents. J. Neurosci. *24*, 5301–5306.

32. Savić, N., Pedarzani, P., and Sciancalepore, M. (2001). Medium afterhyperpolarization and firing pattern modulation in interneurons of stratum radiatum in the CA3 hippocampal region. J. Neurophysiol. *85*, 1986–1997.

33. Zúñiga, R., González, D., Valenzuela, C., Brown, N., and Zúñiga, L. (2016). Expression and cellular localization of HCN channels in rat cerebellar granule neurons. Biochem. Biophys. Res. Commun. *478*, 1429–1435.

34. Nolan, M.F., Malleret, G., Lee, K.H., Gibbs, E., Dudman, J.T., Santoro, B., Yin, D., Thompson, R.F., Siegelbaum, S.A., Kandel, E.R., and Morozov, A. (2003). The hyperpolarization-activated HCN1 channel is important for motor learning and neuronal integration by cerebellar Purkinje cells. Cell *115*, 551–564.

35. Tillotson, R., and Bird, A. (2020). The molecular basis of MeCP2 function in the brain. J. Mol. Biol. *432*, 1602–1623.

36. Li, W., and Pozzo-Miller, L. (2014). BDNF deregulation in Rett syndrome. Neuropharmacology *76*, 737–746.

37. Schmid, D.A., Yang, T., Ogier, M., Adams, I., Mirakhur, Y., Wang, Q., Massa, S.M., Longo, F.M., and Katz, D.M. (2012). A TrkB small molecule partial agonist rescues TrkB phosphorylation deficits and improves respiratory function in a mouse model of Rett syndrome. J. Neurosci. *32*, 1803–1810.

38. Cardenas-Aguayo, M.d.C., Kazim, S.F., Grundke-Iqbal, I., and Iqbal, K. (2013). Neurogenic and neurotrophic effects of BDNF peptides in mouse hippocampal primary neuronal cell cultures. PLoS One *8*, e53596.

39. Krishnan, N., Krishnan, K., Connors, C.R., Choy, M.S., Page, R., Peti, W., Van Aelst, L., Shea, S.D., and Tonks, N.K. (2015). PTP1B inhibition suggests a therapeutic strategy for Rett syndrome. J. Clin. Invest. *125*, 3163–3177.

40. Lindtner, C., Scherer, T., Zielinski, E., Filatova, N., Fasshauer, M., Tonks, N.K., Puchowicz, M., and Buettner, C. (2013). Binge drinking induces whole-body insulin resistance by impairing hypothalamic insulin action. Sci. Transl. Med. *5*, 170ra14.

41. Cheng, T.L., and Qiu, Z. (2014). MeCP2: multifaceted roles in gene regulation and neural development. Neurosci. Bull. *30*, 601–609.

42. Chao, H.T., Zoghbi, H.Y., and Rosenmund, C. (2007). MeCP2 controls excitatory synaptic strength by regulating glutamatergic synapse number. Neuron *56*, 58–65.

43. Della Sala, G., and Pizzorusso, T. (2014). Synaptic plasticity and signaling in Rett syndrome. Dev. Neurobiol. *74*, 178–196.

44. Blackman, M.P., Djukic, B., Nelson, S.B., and Turrigiano, G.G. (2012). A critical and cell-autonomous role for MeCP2 in synaptic scaling up. J. Neurosci. *32*, 13529–13536.

45. Qiu, Z., Sylwestrak, E.L., Lieberman, D.N., Zhang, Y., Liu, X.Y., and Ghosh, A. (2012). The Rett syndrome protein MeCP2 regulates synaptic scaling. J. Neurosci. *32*, 989–994.

46. Zhong, X., Li, H., and Chang, Q. (2012). MeCP2 phosphorylation is required for modulating synaptic scaling through mGluR5. J. Neurosci. *32*, 12841–12847.

47. Johnson, B.S., Zhao, Y.T., Fasolino, M., Lamonica, J.M., Kim, Y.J., Georgakilas, G., Wood, K.H., Bu, D., Cui, Y., Goffin, D., et al. (2017). Biotin tagging of MeCP2 in mice reveals contextual insights into the Rett syndrome transcriptome. Nat. Med. *23*, 1203–1214.

48. Chen, W.G., Chang, Q., Lin, Y., Meissner, A., West, A.E., Griffith, E.C., Jaenisch, R., and Greenberg, M.E. (2003). Derepression of BDNF transcription involves calcium-dependent phosphorylation of MeCP2. Science *302*, 885–889.

49. Martinowich, K., Hattori, D., Wu, H., Fouse, S., He, F., Hu, Y., Fan, G., and Sun, Y.E. (2003). DNA methylation-related chromatin remodeling in activity-dependent BDNF gene regulation. Science *302*, 890–893.

50. Klein, M.E., Lioy, D.T., Ma, L., Impey, S., Mandel, G., and Goodman, R.H. (2007). Homeostatic regulation of MeCP2 expression by a CREB-induced microRNA. Nat. Neurosci. *10*, 1513–1514.

51. Chahrour, M., Jung, S.Y., Shaw, C., Zhou, X., Wong, S.T.C., Qin, J., and Zoghbi, H.Y. (2008). MeCP2, a key contributor to neurological disease, activates and represses transcription. Science *320*, 1224–1229.

52. Antoine, M.W., Langberg, T., Schnepel, P., and Feldman, D.E. (2019). Increased excitation-inhibition ratio stabilizes synapse and circuit excitability in four autism mouse models. Neuron *101*, 648–661.e4.

53. Ebert, D.H., Gabel, H.W., Robinson, N.D., Kastan, N.R., Hu, L.S., Cohen, S., Navarro, A.J., Lyst, M.J., Ekiert, R., Bird, A.P., and Greenberg, M.E. (2013). Activity-dependent phosphorylation of MeCP2 threonine 308 regulates interaction with NCoR. Nature *499*, 341–345.

54. Lyst, M.J., Ekiert, R., Ebert, D.H., Merusi, C., Nowak, J., Selfridge, J., Guy, J., Kastan, N.R., Robinson, N.D., de Lima Alves, F., et al. (2013). Rett syndrome mutations abolish the interaction of MeCP2 with the NCoR/SMRT co-repressor. Nat. Neurosci. *16*, 898–902.

55. Ren, Y., Barnwell, L.F., Alexander, J.C., Lubin, F.D., Adelman, J.P., Pfaffinger, P.J., Schrader, L.A., and Anderson, A.E. (2006). Regulation of surface localization of the small conductance $Ca^{2+}$-activated potassium channel, Sk2, through direct phosphorylation by cAMP-dependent protein kinase. J. Biol. Chem. *281*, 11769–11779.

56. Koekkoek, S.K.E., Yamaguchi, K., Milojkovic, B.A., Dortland, B.R., Ruigrok, T.J.H., Maex, R., De Graaf, W., Smit, A.E., VanderWerf, F., Bakker, C.E., et al. (2005). Deletion of FMR1 in Purkinje cells enhances parallel fiber LTD, enlarges spines, and attenuates cerebellar eyelid conditioning in Fragile X syndrome. Neuron *47*, 339–352.

57. Baudouin, S.J., Gaudias, J., Gerharz, S., Hatstatt, L., Zhou, K., Punnakkal, P., Tanaka, K.F., Spooren, W., Hen, R., De Zeeuw, C.I., et al. (2012). Shared synaptic pathophysiology in syndromic and nonsyndromic rodent models of autism. Science *338*, 128–132.

58. Zhang, B., Chen, L.Y., Liu, X., Maxeiner, S., Lee, S.J., Gokce, O., and Südhof, T.C. (2015). Neuroligins sculpt cerebellar Purkinje-cell circuits by differential control of distinct classes of synapses. Neuron *87*, 781–796.

59. Ha, S., Lee, D., Cho, Y.S., Chung, C., Yoo, Y.E., Kim, J., Lee, J., Kim, W., Kim, H., Bae, Y.C., et al. (2016). Cerebellar Shank2 regulates excitatory synapse density, motor coordination, and specific repetitive and anxiety-like behaviors. J. Neurosci. *36*, 12129–12143.

60. Schonewille, M., Belmeguenai, A., Koekkoek, S.K., Houtman, S.H., Boele, H.J., van Beugen, B.J., Gao, Z., Badura, A., Ohtsuki, G., Amerika, W.E., et al. (2010). Purkinje cell-specific knockout of the protein phosphatase PP2B impairs potentiation and cerebellar motor learning. Neuron *67*, 618–628.

61. Bina, L., Romano, V., Hoogland, T.M., Bosman, L.W.J., and De Zeeuw, C.I. (2021). Purkinje cells translate subjective salience into readiness to act and choice performance. Cell Rep. *37*, 110116.

62. Yang, C., Tian, Y., Su, F., Wang, Y., Liu, M., Wang, H., Cui, Y., Yuan, P., Li, X., Li, A., et al. (2022). Restoration of FMRP expression in adult V1 neurons rescues visual deficits in a mouse model of fragile X syndrome. Protein Cell *13*, 203–219.

63. Kelly, E., Meng, F., Fujita, H., Morgado, F., Kazemi, Y., Rice, L.C., Ren, C., Escamilla, C.O., Gibson, J.M., Sajadi, S., et al. (2020). Regulation of autism-relevant behaviors by cerebellar-prefrontal cortical circuits. Nat. Neurosci. *23*, 1102–1110.

64. Badura, A., Verpeut, J.L., Metzger, J.W., Pereira, T.D., Pisano, T.J., Deverett, B., Bakshinskaya, D.E., and Wang, S.S.H. (2018). Normal cognitive

and social development require posterior cerebellar activity. Elife *7*, e36401.

65. Yamamoto, M., Kim, M., Imai, H., Itakura, Y., and Ohtsuki, G. (2019). Microglia-triggered plasticity of intrinsic excitability modulates psychomotor behaviors in acute cerebellar inflammation. Cell Rep. *28*, 2923–2938.e8.
66. Barski, J.J., Dethleffsen, K., and Meyer, M. (2000). Cre recombinase expression in cerebellar Purkinje cells. Genesis *28*, 93–98.
67. Zhou, J.H., Wang, X.T., Zhou, L., Zhou, L., Xu, F.X., Su, L.D., Wang, H., Jia, F., Xu, F.Q., Chen, G.Q., et al. (2017). Ablation of TFR1 in Purkinje cells inhibits mGlu1 trafficking and impairs motor coordination, but not autistic-like behaviors. J. Neurosci. *37*, 11335–11352.
68. Wang, X.T., Cai, X.Y., Xu, F.X., Zhou, L., Zheng, R., Ma, K.Y., Xu, Z.H., and Shen, Y. (2019). MEA6 deficiency impairs cerebellar development and motor performance by tethering protein trafficking. Front. Cell. Neurosci. *13*, 250.
69. Wang, R., Tan, J., Guo, J., Zheng, Y., Han, Q., So, K.F., Yu, J., and Zhang, L. (2018). Aberrant development and synaptic transmission of cerebellar cortex in a VPA induced mouse autism model. Front. Cell. Neurosci. *12*, 500.
70. Shen, Y., and Linden, D.J. (2005). Long-term potentiation of neuronal glutamate transporters. Neuron *46*, 715–722.
71. Su, L.D., and Shen, Y. (2009). Blockade of glutamate transporters facilitates cerebellar synaptic long-term depression. Neuroreport *20*, 502–507.
72. Zhou, L., Yang, D., Wang, D.J., Xie, Y.J., Zhou, J.H., Zhou, L., Huang, H., Han, S., Shao, C.Y., Li, H.S., et al. (2015). Numb deficiency in cerebellar Purkinje cells impairs synaptic expression of metabotropic glutamate receptor and motor coordination. Proc. Natl. Acad. Sci. USA *112*, 15474–15479.
73. Tian, J., Tep, C., Benedick, A., Saidi, N., Ryu, J.C., Kim, M.L., Sadasivan, S., Oberdick, J., Smeyne, R., Zhu, M.X., and Yoon, S.O. (2014). p75 regulates Purkinje cell firing by modulating SK channel activity through Rac1. J. Biol. Chem. *289*, 31458–31472.
74. Shimizu, H., and Yamanouchi, K. (2011). Acceleration of irregular estrous cycle in forced running by midbrain raphe lesions in female rats. Neurosci. Lett. *495*, 192–195.
75. Navarro, M., Rodríguez de Fonseca, F., Hernández, M.L., Ramos, J.A., and Fernández-Ruiz, J.J. (1994). Motor behavior and nigrostriatal dopaminergic activity in adult rats perinatally exposed to cannabinoids. Pharmacol. Biochem. Behav. *47*, 47–58.
76. Silverman, J.L., Babineau, B.A., Oliver, C.F., Karras, M.N., and Crawley, J.N. (2013). Influence of stimulant-induced hyperactivity on social approach in the BTBR mouse model of autism. Neuropharmacology *68*, 210–222.

## STAR★METHODS

### KEY RESOURCES TABLE

| REAGENT or RESOURCE | SOURCE | IDENTIFIER |
|---|---|---|
| Antibodies | | |
| Rabbit polyclonal, anti-mGluR1 | BD Biosciences | Cat# 610965, RRID: AB_398278 |
| Rabbit polyclonal, anti-flotillin | BD Biosciences | Cat# 610820, RRID: AB_398139 |
| Rabbit polyclonal, anti-PSD95 | Millipore | Cat# MAB1598, RRID: AB_94278 |
| Rabbit polyclonal, anti-GAPDH | Millipore | Cat# MAB374, RRID: AB_2107445 |
| Rabbit polyclonal, anti-GluA2 | Millipore | Cat# MAB397, RRID: AB_2113875 |
| Rabbit polyclonal, anti-MeCP2 | Abcam | Cat# ab2828, RRID: AB_2143853 |
| Rabbit polyclonal, anti-EAAT4 | Alpha Diagnostics | Cat# EAAT41-A, RRID: AB_1622384 |
| Rabbit polyclonal, anti-Flag | Abmart | Cat# M20018, RRID: AB_2936247 |
| Rabbit polyclonal, anti-TrkB | Cell Signaling | Cat# 4603, RRID: AB_2155125 |
| Rabbit polyclonal, anti-TrkB-pY706 | Affinity Biosciences | Cat# AF3461, RRID: AB_2834899 |
| Rabbit polyclonal, anti-SK2 | Alomone | Cat# APC-028, RRID: AB_2040126 |
| Goat anti-Mouse IgG (H + L) Secondary Antibody, HRP | Thermo Fisher | Cat# 31430, RRID:AB_228307 |
| Goat anti-Rabbit IgG (H + L) Secondary Antibody, HRP | Thermo Fisher | Cat# 31460, RRID:AB_228341 |
| Goat anti-Rabbit IgG (H + L) Cross-Adsorbed Secondary Antibody, Alexa Fluor™ 488 | Invitrogen | Cat# A-11008, RRID:AB_143165 |
| Goat anti-Mouse IgG (H + L) Cross-Adsorbed Secondary Antibody, Alexa Fluor™ 488 | Invitrogen | Cat# A-11001, RRID:AB_2534069 |
| Goat anti-Mouse IgG (H + L) Cross-Adsorbed Secondary Antibody, Alexa Fluor™ 594 | Invitrogen | Cat# A-11005, RRID:AB_2534073 |
| Bacterial and virus strains | | |
| AAV9-DIO-eGFP-TrkB-Y706E-Flag | Shengbo, Shanghai | N/A |
| Chemicals, peptides, and recombinat proteins | | |
| Nissl | Beyotime, Shanghai | Cat# C0117 |
| Protease inhibitor cocktail | Merck Chemicals | Cat# 4693132001 |
| ProLong™ Gold Antifade Mountant with DAPI | Invitrogen | Cat# P36941 |
| EZ-link-sulfo-NHS-SS-Biotin | Thermo Fisher | Cat# 21331 |
| SDS | Sigma-Merck | Cat# 28365 |
| Triton X-100 | Sigma-Merck | Cat# 85111 |
| CPT-157633 | MedChemExpress | Cat# HY111469 |
| Streptavidin agarose | Thermo Fisher | Cat# 20349 |
| NBQX | Tocris Bioscience | Cat# 0373/10 |
| Apamin | MCE | Cat# HY-P0256 |
| TEA | Tocris Bioscience | Cat# 3068/50 |
| Gabazine | Tocris Bioscience | Cat# 1262/10 |
| Adhesive | 3M | Cat# 41453 |
| TTX | Abcam | Cat# ab120055 |
| Critical commercial assays | | |
| BCA protein assay kit | Tiangen | Cat# PA115 |
| OneStep Kit | Qiagen | Cat# 210212 |
| PVDF membrane | Sigma-Merck | Cat# IPVH00010 |
| enhanced chemiluminescence | Pierce Biotechnology | Cat# 32106 |
| Rapid Golgi Stain kit | FD Neuro Tech Inc. | Cat# PK401 |

(*Continued on next page*)

*Continued*

| REAGENT or RESOURCE | SOURCE | IDENTIFIER |
|---|---|---|
| Experimental models: Organisms/strains | | |
| *Mecp2*$^{f/+}$ mice | Dr. Zi-Long Qiu from Chinese Academy of Sciences, Shanghai | N/A |
| *Pcp2*-Cre mice | Jackson Laboratory | Cat# 006207, RRID:IMSR_JAX:006209 |
| Oligonucleotides | | |
| *Mecp2* forward primer: CAGGCAAAGCAGAGACATCA | Thermo Fisher | N/A |
| *Mecp2* reverse primer: GCTTAAGCTTCCGTGTCCAG | Thermo Fisher | N/A |
| *Calbindin* forward primer: GGCTTCATTTCGACGCTGAC | Thermo Fisher | N/A |
| *Calbindin* reverse primer: ACGTGAGCCAACTCTACAATTC | Thermo Fisher | N/A |
| *Gapdh* forward primer: GGTGAAGGTCGGTGTGAACG | Thermo Fisher | N/A |
| *Gapdh* reverse primer: CTCGCTCCTGGAAGATGGTG | Thermo Fisher | N/A |
| Software and algorithms | | |
| Igor Pro 6.0 | Wavemetrics | RRID:SCR_000325 |
| Graphpad Prism | Graphpad software | RRID:SCR_002798 |
| SPSS 16.0 | IBM | RRID:SCR_002865 |
| ImageJ 1.42q | NIH | RRID:SCR_003070 |
| NeuroLucida software | MBF Bioscience | RRID:SCR_001775 |
| ANY-maze video tracking | Stoelting Co. | RRID:SCR_014289 |
| MATLAB analysis | Mathwork | RRID:SCR_001622 |
| Eye-tracking software | ISCAN systems | ETL-200 |

## RESOURCE AVAILABILITY

### Lead contact

Further information and requests for resources and reagents should be directed to and will be fulfilled by the Lead Contact, Ying Shen (yshen@zju.edu.cn).

### Materials availability

This study did not generate new unique reagents.

### Data and code availability

- Electrophysiology and behavior data reported in this paper will be shared by the lead contact upon request.
- This paper does not report original code.
- Any additional information required to reanalyze the data reported in this paper is available from the lead contact upon request.

## EXPERIMENTAL MODEL AND STUDY PARTICIPANT DETAILS

### Mouse

All animal experiments were carried out in a strict compliance with protocols approved by the Animal Care and Use Committee at Zhejiang University School of Medicine. Mice were kept under temperature-controlled conditions on a 12:12 h light/dark cycle with food and water *ad libitum*. Original *Mecp2*$^{f/+}$ mice were kindly provided by Zi-Long Qiu. Conditioned knockout mice were obtained by crossing *Mecp2*$^{f/+}$ mice with *Pcp2*-Cre mice obtained from Jackson Laboratory (#006207).[66,67] To determine the role of MeCP2, mice with *Mecp2* deletion specifically in PCs (pCre;*Mecp2*$^{f/f}$ and pCre;*Mecp2*$^{f/y}$) were generated by crossing *Pcp2*-Cre with *Mecp2*$^{f/f}$ (female) or *Mecp2*$^{f/y}$ (male) mice, respectively. The resulting offspring were genotyped by PCR assays using their tail DNA.

## METHOD DETAILS

### RT-PCR

The contents of 10 PCs were harvested as described in previous work.[67,68] The harvested contents were subjected to RT-PCR using OneStep Kit (Qiagen, Germantown, MD). Forward (F) and reverse (R) primers used for amplification were: *Mecp2*, F:5′- CAG GCA AAG CAG AGA CAT CA -3'; R:5′- GCT TAA GCT TCC GTG TCC AG -3'; *Calbindin*, F:5′-GGC TTC ATT TCG ACG CTG AC-3';

R:5′-ACG TGA GCC AAC TCT ACA ATT C-3’; *Gapdh*, F:5′-GGT GAA GGT CGG TGT GAA CG -3’; R:5′-CTC GCT CCT GGA AGA TGG TG-3’.

### Surface biotinylation

Acute slices were incubated in aCSF with 0.5 mg/mL EZ-link-sulfo-NHS-SS-Biotin (21331; Thermo Fisher, Waltham, MA) for 30 min, and then washed with ice-cold PBS and lysed with a radioimmunoprecipitation assay buffer [1% Triton X-100, 0.5% deoxycholate, 0.2% SDS, 100 mM NaCl, 1 mM EDTA, 50 mM Tris-HCl (pH 7.4)] supplemented with protease inhibitors. Biotinylated proteins were separated using streptavidin agarose (20349; Thermo Fisher) overnight at 4°C. The beads were washed three times with immunoprecipitation assay buffer, and the biotinylated proteins were eluted with 2× SDS sample buffer.

### Western blotting

Cerebellar tissues were rinsed with PBS and diluted in 1% SDS containing protease inhibitors. After determining protein concentration with BCA protein assay (Bio-Rad, Hercules, CA), equal quantities of proteins were loaded and fractionated on SDS-PAGE and transferred to PVDF membrane (Immobilon-P, Sigma-Merck), immunoblotted with antibodies, and visualized by enhanced chemiluminescence (Pierce Biotechnology). Primary antibody dilutions were mGluR1 (1:5,000), GluA2 (1:2,000), EAAT4 (1:5,000), PSD95 (1:10,000), calbindin (1:10,000), Flag (1:10,000), SK2 (1:1,000), TrkB (1:1,000), TrkB-pY706 (1:1,000), flotillin (1:2,000), GAPDH (1:40,000), and secondary antibodies (1:10,000). Film signals were digitally scanned and quantitated using ImageJ 1.42q.

### Immunohistochemistry

20-μm sagittal sections from mice were prepared and placed in blocking solution for 1 h at room temperature (RT). After washing with PBS, sections were incubated with primary antibodies overnight at 4°C and incubated with secondary antibodies for 1 h at RT. Primary antibody dilutions used for immunohistochemistry were *Mecp2* (1:200), and calbindin (1:1,000), and secondary antibodies (1:1,000). Immunohistochemical images were obtained with a confocal microscope (Olympus, Tokyo) and the parameters used in microscopy were consistent in all experiments.

### Nissl staining

Sagittal cerebellar slices (30 μm) were immersed in Nissl staining solution (Beyotime, Shanghai) for 5 min, rinsed with distilled water, dehydrated in ethanol, and cleared in xylene. Images of cerebellar cortex were captured using a light microscope.

### Golgi staining and sholl analysis

Golgi staining was performed using Rapid Golgi Stain Kit (FD NeuroTech Inc., Ellicott City, MD) according to the standard procedure. PCs at the apical region were imaged using a bright field microscope (Zeiss, Germany). NeuroLucida software (MBF Bioscience, Williston, VT) was used to plot the soma and dendrites of the PCs under a manually assisted mode. Sholl analysis was adopted according to previous work.[69] A series of concentric circles (10 μm interval) were plotted around the soma. The number of intersections of dendrites for each circle and the dendrite length within each 10 μm segment were quantified using NeuroLucida software.

### Recombinant virus and *in vivo* injection

To express $TrkB^{Y706E}$ in PCs, recombinant AAV9 was constructed in combination with enhanced GFP (eGFP) and Flag. Under deep anesthesia with an intraperitoneal injection of 0.7% pentobarbital sodium (10 μL/g), a viral solution (300 nL) containing recombinant AAV9 (2.3E12 FFU/ml) was injected into lobules V-VI of cerebellar vermis of pCre;$Mecp2^{f/y}$ mice (P30) at a rate of 30 nL/min using a glass pipette (30 μm in diameter) and a microinjector (World Precision Instruments, Sarasota, FL). The injected animals were decapitated 2 months later and eGFP signals were observed in affected lobules.

### Electrophysiology

Sagittal slices of cerebellar vermis (250 μm) were prepared from anesthetized mice using a vibrating tissue slicer (Leica VT1000S, Germany) and ice-cold aCSF containing (in mM): 125 NaCl, 2.5 KCl, 1.25 $NaH_2PO_4$, 1 $MgCl_2$, 2 $CaCl_2$, 26 $NaHCO_3$ and 25 D-glucose, bubbled with 95% $O_2$/5% $CO_2$. After recovery for 30 min at 35°C, slices were placed in a submerged chamber that was perfused at 2 mL/min with aCSF.

Patch clamp electrodes (3–5 MΩ) were filled with an intracellular solution composed of either (in mM) 135 Cs-methanesulfonate, 10 CsCl, 10 HEPES, 0.2 EGTA, 4 $Na_2$ATP, and 0.4 $Na_3$GTP (pH 7.3, OSM 290) for voltage-clamp recording; or (in mM) 134 K-gluconate, 6 KCl, 4 NaCl, 10 HEPES, 0.2 EGTA, 4 $Na_2$ATP, 0.3 $Na_3$GTP, and 14 $Na_2$phosphocreatine (pH 7.3, OSM 290) for current-clamp recording; or (in mM): 150 Cs-methanesulfonate, 5 KCl, 0.1 EGTA, 5 HEPES, 3 MgATP, and 0.4 $Na_3$GTP (pH 7.3, OSM 290) for recording IPSCs (5–7); or (in mM) 135 K-gluconate, 10 KCl, 1 $MgCl_2$, 2 $Na_2$-ATP, 0.4 $Na_3$-GTP, 10 HEPES (pH 7.3, OSM 290) for recording SK and tail currents.

PCs were visualized under an upright microscope (BX51, Olympus, Tokyo, Japan) with a 40× water-immersion objective and equipped with infrared differential interference contrast enhancement. Whole-cell recordings were obtained with an Axon MultiClamp 700B amplifier (Molecular Devices, Foster City, CA). Currents were digitized at 10 kHz and low-pass filtered at 3 kHz. To acquire PF-EPSCs, standard patch pipettes were filled with aCSF and placed in the middle third of molecular layer with aCSF

containing Gabazine (10 μM). PF-EPSCs were evoked using ~4 μA pulses (100 μs). To acquire eIPSCs, stimulation electrodes were placed in the inner fourth of molecular layer with aCSF containing NBQX (5 μM). To record CF-EPSCs, a constant current step (3–30 μA) was applied to a patch pipette that was positioned in granule cell layer close to the vicinity of recorded neuron. The recording was performed at a holding potential of −10 mV, while stimulus intensity and electrode position were adjusted so that an all-or-none response was elicited[70,71]. Recordings were excluded from analysis if the series or input resistance varied by > 15% over the course of an experiment. EPSCs and IPSCs were measured with equal driving force, excitatory/inhibitory input ratio was calculated from EPSCs and IPSCs as E/(E + I).

mEPSCs and mIPSCs were recorded in whole-cell configuration in the presence of 0.5 μM tetrodotoxin (TTX) plus Gabazine (10 μM) or NBQX, respectively. The offline analysis of mEPSCs and mIPSCs was conducted using a sliding template algorithm (ClampFit 10, Molecular Device). The criteria for inclusion were 1) an amplitude larger than 6 pA and 2) a rise time (10–90%) longer than 1 ms. Overlapping events were rejected. mGluR1 currents were recorded by driving PCs using a burst PF stimulation (100 Hz) under a holding voltage of −70 mV in aCSF plus NBQX.[72]

To record input-output curves, the membrane voltage of clamped cells was set at approximately −70 mV. A series of current steps was delivered to PCs with an interval of 30 s. AP amplitude was measured from the threshold to the peak. AP width was measured at half amplitude. AHP was measured from AP threshold to the negative peak. AP threshold was measured in the first derivative of action potential ($dV/dt$) where the velocity was close to 50 mV/ms.

SK2 and tail currents were recorded using a protocol according to previous work.[73] To record SK currents, slices were perfused with aCSF supplemented with 1 μM TTX, 1 mM TEA, and/or apamin (100 nM) in the bath perfusion, and PCs were held at −80 mV before stepping to potentials. The steady currents within the duration of 2 ms before the end of steps were measured (gray column) as SK2 currents. To record tail currents, slices were perfused with aCSF containing 1 μM TTX and 1 mM TEA and PCs were held at −50 mV for 50 ms before stepping to potentials between −40 mV and 30 mV (10 mV/step, 100-ms duration, 30-s interval).

### Footprint test

Walking gait was tested according to previous work.[67,68] With hind paws painted with ink, mice were allowed to freely traverse a clear plexiglass tunnel (100 cm × 10 cm × 10 cm, length × width × height), with a sheet of white absorbent paper (100 cm × 10 cm, length × width) placed on the ground. A darkened cage was placed at the end of the tunnel, encouraging mice to run toward the safe environment. The resulting tracks provided a spatial relationship of consecutive foot prints, from which stride length and stance width were measured. Three step cycles were averaged, with each cycle considered as the distance from one pair of prints to the next.

### Rotarod test

After habituation at 5 rpm to the rotarod, control and cKO mice were tested for eight consecutive days. In each session, the velocity of the rotation increased with a constant acceleration of 9 rpm/min$^2$ from 5 rpm to 50 rpm. Only male offspring were used in rotarod and compensatory eye movement tests, because the performance of female mice depends on the phase of estrous cycle, which may affect chronic motor training and confound the results.[74]

### Three chamber test

The apparatus consisted of a rectangular plexiglas box (60 cm × 35 cm × 3 cm, length × width × height) evenly divided into three chambers. Age- and gender-matched WT target subjects (S1 and S2) were habituated for 5 consecutive days before the test by being placed inside metal-wired cages. On the test day, test mice were placed in the central chamber for 10-min habituation. S1 was introduced into a wire cage in one chamber and the empty chamber served as an inanimate object with no social valence. The dividers were then raised to allow test mice to freely explore all three chambers over a 10-min session. The time spent in each chamber was recorded and the ratio of (S1-E) to (S1+E) was calculated as the preference index (S1-E). Subsequently, S2 was immediately introduced to the other chamber. Again, test mice spent another 10 min in exploring the entire apparatus. Total time spent in each chamber was recorded and the ratio of (S2-S1) to (S2+S1) was measured as the preference index (S2-S1). Behavioral videos were recorded using ANY-maze video tracking system (Stoelting Co.).

### Grooming test

Spray-induced grooming was performed according to previous work.[75] Each mouse was placed individually into a standard cage (45 × 45 × 50 cm), which was empty to eliminate digging, for a 5 min habituation and then misted from above with water (23°C) for one time using a manual spraying device. The spray adequately coated the dorsal surface of mouse with mist. The activity of mouse was then recorded for 10 min with a high-speed camera (30 Hz frame rate) and analyzed by a trained observer. Cumulative time and bouts of grooming were scored from the videos as previously described.[76]

### Marble burying test

A clean cage (50 × 26 × 18 cm) was filled with 4-cm-depth bedding material and 20 glass marbles. The marbles were arranged in an equidistant 4 × 5 grid. Animals were given access to the marbles for 30 min. After 30 min, the burying of marbles was scored. The score was 1 when a marble was 100% covered or 0.5 when it was just partially covered. All scores were assessed by two independent researchers.

### T-maze test

Mice were placed in a T-maze with two arms (50 cm length) and allowed to freely explore either arm for 10 consecutive trials. A choice was counted when the mouse stepped into one arm with four paws. The gate to that arm was immediately closed and the mouse was allowed to explore there for 5 s. The mouse was then gently placed back to the base for next trial. If the mouse selected the same arm in two consecutive trials, this was scored as one repeat.

### Resident-intruder test

Male mice (4 weeks old) were used as stimulus mice. The test was performed in a home cage of a test mouse and began when a stimulus mouse was introduced to the cage. The test mouse was allowed to explore stimulus mouse for 5 min (trial 1), then the stimulus mouse was removed. After an inter-trial interval of 1 h, the test mouse was re-exposed original (the stimulus mouse in trial 1) or a novel stimulus mouse for another 5 min (trial 2). All social behaviors (body sniffing, anogenital and nose-to-nose sniffing, following, and allogrooming) initiated by test subject in the first 1 min in trial 1 and trial 2 was measured. The difference score was calculated by subtracting the time spent in social interaction during trial 2 from the social interaction time during trial 1. The behavioral were recorded using ANY-maze.

### Olfactory habituation test

This test consists of sequential presentations of two odors using the cotton swabs: banana and almond. Each odor was presented three times for a duration of 2 min with an inter-trial interval being 1 min. The investigation of swabs was recorded using a stopwatch.

### Compensatory eye movement

A small immobilizing construct (pedestal) was attached to mouse's skull using an adhesive (Kerr, Bioggio, Switzerland). The pedestal consisted of a brass holder with a neodymium magnet and a screw hole for fixation. After recovery, mice were head-restrained by fixation using the pedestal. A round screen with a random dotted pattern ('drum') surrounded the mouse during the experiment. OKR, VOR and VVOR were induced using a sinusoidal rotation of the drum in light (OKR), rotation of the table in the dark (VOR) or the rotation of the table (VVOR) in the light. Motor behavior was assessed by rotating the table and/or drum at various oscillation frequencies, ranging from 0.1 to 1.0 Hz with a fixed 5° amplitude. To evaluate motor learning, a mismatch between visual and vestibular input was created. Rotating both visual and vestibular stimuli in phase (at the same amplitude of 5°, at 0.6 Hz) induced a decrease of gain (day 1). Subsequently, rotating the drum at greater amplitude relative to the table induced phase reversal of VOR (all days table rotation 5°; day 2, drum amplitude 7.5°; day 3–5, drum amplitude 10°). For eye illumination during the experiments, two table-fixed infrared emitters (output 600 mW, dispersion angle 7°, peak wavelength 880 nm) and a third emitter, which produced the tracked corneal reflection and was aligned horizontally with the optical axis of the camera, were mounted to the camera. Eye movements were recorded with eye-tracking software (ETL-200, ISCAN systems, Burlington, NA). Gain and phase values of eye movements were calculated using custom made MATLAB analysis routines.

## QUANTIFICATION AND STATISTICAL ANALYSIS

Experimenters who performed experiments and analyses were blinded to the genotypes until all data were integrated. Data were analyzed using Igor Pro 6.0 (Wavemetrics, Lake Oswego, OR), Graphpad Prism (San Diego, CA) and SPSS 16.0 (IBM, Chicago, IL). No statistical methods were used to pre-determine sample sizes, which were based on our previous studies. All datasets were tested for the assumptions of normality of distribution. Statistical differences were determined using unpaired two-sided Student's t-test for two-group comparison, or one-way ANOVA followed by LSD's *post hoc* test for multiple comparisons, or repeated measures ANOVA for repeated measures. The level for significance was set at $p < 0.05$. "*n*" represents the number of animals, cells or batches depending on experiments. Data in the text and figures are presented as the mean ± SD or mean ± SEM. For correlation test, linear regression lines were created using Excel algorithm. SPSS was used to analyze the covariant correlation between the slopes of two regression lines, for which the univariate-dependent general linear model was selected and current injection was set as the fixed factor.